EUROPEAN LABORATORY FOR PARTICLE PHYSICS

CERN-EP/98-108
3rd July 1998

Tests of the Standard Model and Constraints on New Physics from Measurements of Fermion-pair Production at 183 GeV at LEP

The OPAL Collaboration

Abstract

Cross-sections for hadronic, $b\overline{b}$ and lepton pair final states in e^+e^- collisions at $\sqrt{s}$=183 GeV, measured with the OPAL detector at LEP, are presented and compared with the predictions of the Standard Model. Forward-backward asymmetries for the leptonic final states have also been measured. Cross-sections and asymmetries are also presented for data recorded in 1997 at $\sqrt{s}$=130 and 136 GeV. The results are used to measure the energy dependence of the electromagnetic coupling constant $\alpha_{\rm em}$, and to place limits on new physics as described by four-fermion contact interactions or by the exchange of a new heavy particle such as a leptoquark, or of a squark or sneutrino in supersymmetric theories with R-parity violation.

Submitted to Eur. Phys. J. C

The OPAL Collaboration

G. Abbiendi[2], K. Ackerstaff[8], G. Alexander[23], J. Allison[16], N. Altekamp[5], K.J. Anderson[9], S. Anderson[12], S. Arcelli[17], S. Asai[24], S.F. Ashby[1], D. Axen[29], G. Azuelos[18,a], A.H. Ball[17], E. Barberio[8], R.J. Barlow[16], R. Bartoldus[3], J.R. Batley[5], S. Baumann[3], J. Bechtluft[14], T. Behnke[27], K.W. Bell[20], G. Bella[23], A. Bellerive[9], S. Bentvelsen[8], S. Bethke[14], S. Betts[15], O. Biebel[14], A. Biguzzi[5], S.D. Bird[16], V. Blobel[27], I.J. Bloodworth[1], M. Bobinski[10], P. Bock[11], J. Böhme[14], D. Bonacorsi[2], M. Boutemeur[34], S. Braibant[8], P. Bright-Thomas[1], L. Brigliadori[2], R.M. Brown[20], H.J. Burckhart[8], C. Burgard[8], R. Bürgin[10], P. Capiluppi[2], R.K. Carnegie[6], A.A. Carter[13], J.R. Carter[5], C.Y. Chang[17], D.G. Charlton[1,b], D. Chrisman[4], C. Ciocca[2], P.E.L. Clarke[15], E. Clay[15], I. Cohen[23], J.E. Conboy[15], O.C. Cooke[8], C. Couyoumtzelis[13], R.L. Coxe[9], M. Cuffiani[2], S. Dado[22], G.M. Dallavalle[2], R. Davis[30], S. De Jong[12], L.A. del Pozo[4], A. de Roeck[8], K. Desch[8], B. Dienes[33,d], M.S. Dixit[7], J. Dubbert[34], E. Duchovni[26], G. Duckeck[34], I.P. Duerdoth[16], D. Eatough[16], P.G. Estabrooks[6], E. Etzion[23], H.G. Evans[9], F. Fabbri[2], M. Fanti[2], A.A. Faust[30], F. Fiedler[27], M. Fierro[2], I. Fleck[8], R. Folman[26], A. Fürtjes[8], D.I. Futyan[16], P. Gagnon[7], J.W. Gary[4], J. Gascon[18], S.M. Gascon-Shotkin[17], G. Gaycken[27], C. Geich-Gimbel[3], G. Giacomelli[2], P. Giacomelli[2], V. Gibson[5], W.R. Gibson[13], D.M. Gingrich[30,a], D. Glenzinski[9], J. Goldberg[22], W. Gorn[4], C. Grandi[2], E. Gross[26], J. Grunhaus[23], M. Gruwé[27], G.G. Hanson[12], M. Hansroul[8], M. Hapke[13], K. Harder[27], C.K. Hargrove[7], C. Hartmann[3], M. Hauschild[8], C.M. Hawkes[5], R. Hawkings[27], R.J. Hemingway[6], M. Herndon[17], G. Herten[10], R.D. Heuer[8], M.D. Hildreth[8], J.C. Hill[5], S.J. Hillier[1], P.R. Hobson[25], A. Hocker[9], R.J. Homer[1], A.K. Honma[28,a], D. Horváth[32,c], K.R. Hossain[30], R. Howard[29], P. Hüntemeyer[27], P. Igo-Kemenes[11], D.C. Imrie[25], K. Ishii[24], F.R. Jacob[20], A. Jawahery[17], H. Jeremie[18], M. Jimack[1], C.R. Jones[5], P. Jovanovic[1], T.R. Junk[6], D. Karlen[6], V. Kartvelishvili[16], K. Kawagoe[24], T. Kawamoto[24], P.I. Kayal[30], R.K. Keeler[28], R.G. Kellogg[17], B.W. Kennedy[20], A. Klier[26], S. Kluth[8], T. Kobayashi[24], M. Kobel[3,e], D.S. Koetke[6], T.P. Kokott[3], M. Kolrep[10], S. Komamiya[24], R.V. Kowalewski[28], T. Kress[11], P. Krieger[6], J. von Krogh[11], T. Kuhl[3], P. Kyberd[13], G.D. Lafferty[16], D. Lanske[14], J. Lauber[15], S.R. Lautenschlager[31], I. Lawson[28], J.G. Layter[4], D. Lazic[22], A.M. Lee[31], D. Lellouch[26], J. Letts[12], L. Levinson[26], R. Liebisch[11], B. List[8], C. Littlewood[5], A.W. Lloyd[1], S.L. Lloyd[13], F.K. Loebinger[16], G.D. Long[28], M.J. Losty[7], J. Ludwig[10], D. Liu[12], A. Macchiolo[2], A. Macpherson[30], W. Mader[3], M. Mannelli[8], S. Marcellini[2], C. Markopoulos[13], A.J. Martin[13], J.P. Martin[18], G. Martinez[17], T. Mashimo[24], P. Mättig[26], W.J. McDonald[30], J. McKenna[29], E.A. Mckigney[15], T.J. McMahon[1], R.A. McPherson[28], F. Meijers[8], S. Menke[3], F.S. Merritt[9], H. Mes[7], J. Meyer[27], A. Michelini[2], S. Mihara[24], G. Mikenberg[26], D.J. Miller[15], R. Mir[26], W. Mohr[10], A. Montanari[2], T. Mori[24], K. Nagai[8], I. Nakamura[24], H.A. Neal[12], B. Nellen[3], R. Nisius[8], S.W. O'Neale[1], F.G. Oakham[7], F. Odorici[2], H.O. Ogren[12], M.J. Oreglia[9], S. Orito[24], J. Pálinkás[33,d], G. Pásztor[32], J.R. Pater[16], G.N. Patrick[20], J. Patt[10], R. Perez-Ochoa[8], S. Petzold[27], P. Pfeifenschneider[14], J.E. Pilcher[9], J. Pinfold[30], D.E. Plane[8], P. Poffenberger[28], J. Polok[8], M. Przybycień[8], C. Rembser[8], H. Rick[8], S. Robertson[28], S.A. Robins[22], N. Rodning[30], J.M. Roney[28], K. Roscoe[16], A.M. Rossi[2], Y. Rozen[22], K. Runge[10], O. Runolfsson[8], D.R. Rust[12], K. Sachs[10], T. Saeki[24], O. Sahr[34], W.M. Sang[25], E.K.G. Sarkisyan[23], C. Sbarra[29], A.D. Schaile[34], O. Schaile[34], F. Scharf[3], P. Scharff-Hansen[8], J. Schieck[11], B. Schmitt[8], S. Schmitt[11], A. Schöning[8], M. Schröder[8], M. Schumacher[3], C. Schwick[8], W.G. Scott[20], R. Seuster[14], T.G. Shears[8], B.C. Shen[4], C.H. Shepherd-Themistocleous[8], P. Sherwood[15], G.P. Siroli[2], A. Sittler[27], A. Skuja[17], A.M. Smith[8], G.A. Snow[17], R. Sobie[28], S. Söldner-Rembold[10],

M. Sproston[20], A. Stahl[3], K. Stephens[16], J. Steuerer[27], K. Stoll[10], D. Strom[19], R. Ströhmer[34], B. Surrow[8], S.D. Talbot[1], S. Tanaka[24], P. Taras[18], S. Tarem[22], R. Teuscher[8], M. Thiergen[10], M.A. Thomson[8], E. von Törne[3], E. Torrence[8], S. Towers[6], I. Trigger[18], Z. Trócsányi[33], E. Tsur[23], A.S. Turcot[9], M.F. Turner-Watson[8], R. Van Kooten[12], P. Vannerem[10], M. Verzocchi[10], H. Voss[3], F. Wäckerle[10], A. Wagner[27], C.P. Ward[5], D.R. Ward[5], P.M. Watkins[1], A.T. Watson[1], N.K. Watson[1], P.S. Wells[8], N. Wermes[3], J.S. White[6], G.W. Wilson[16], J.A. Wilson[1], T.R. Wyatt[16], S. Yamashita[24], G. Yekutieli[26], V. Zacek[18], D. Zer-Zion[8]

[1]School of Physics and Astronomy, University of Birmingham, Birmingham B15 2TT, UK
[2]Dipartimento di Fisica dell' Università di Bologna and INFN, I-40126 Bologna, Italy
[3]Physikalisches Institut, Universität Bonn, D-53115 Bonn, Germany
[4]Department of Physics, University of California, Riverside CA 92521, USA
[5]Cavendish Laboratory, Cambridge CB3 0HE, UK
[6]Ottawa-Carleton Institute for Physics, Department of Physics, Carleton University, Ottawa, Ontario K1S 5B6, Canada
[7]Centre for Research in Particle Physics, Carleton University, Ottawa, Ontario K1S 5B6, Canada
[8]CERN, European Organisation for Particle Physics, CH-1211 Geneva 23, Switzerland
[9]Enrico Fermi Institute and Department of Physics, University of Chicago, Chicago IL 60637, USA
[10]Fakultät für Physik, Albert Ludwigs Universität, D-79104 Freiburg, Germany
[11]Physikalisches Institut, Universität Heidelberg, D-69120 Heidelberg, Germany
[12]Indiana University, Department of Physics, Swain Hall West 117, Bloomington IN 47405, USA
[13]Queen Mary and Westfield College, University of London, London E1 4NS, UK
[14]Technische Hochschule Aachen, III Physikalisches Institut, Sommerfeldstrasse 26-28, D-52056 Aachen, Germany
[15]University College London, London WC1E 6BT, UK
[16]Department of Physics, Schuster Laboratory, The University, Manchester M13 9PL, UK
[17]Department of Physics, University of Maryland, College Park, MD 20742, USA
[18]Laboratoire de Physique Nucléaire, Université de Montréal, Montréal, Quebec H3C 3J7, Canada
[19]University of Oregon, Department of Physics, Eugene OR 97403, USA
[20]CLRC Rutherford Appleton Laboratory, Chilton, Didcot, Oxfordshire OX11 0QX, UK
[22]Department of Physics, Technion-Israel Institute of Technology, Haifa 32000, Israel
[23]Department of Physics and Astronomy, Tel Aviv University, Tel Aviv 69978, Israel
[24]International Centre for Elementary Particle Physics and Department of Physics, University of Tokyo, Tokyo 113, and Kobe University, Kobe 657, Japan
[25]Institute of Physical and Environmental Sciences, Brunel University, Uxbridge, Middlesex UB8 3PH, UK
[26]Particle Physics Department, Weizmann Institute of Science, Rehovot 76100, Israel
[27]Universität Hamburg/DESY, II Institut für Experimental Physik, Notkestrasse 85, D-22607 Hamburg, Germany
[28]University of Victoria, Department of Physics, P O Box 3055, Victoria BC V8W 3P6, Canada
[29]University of British Columbia, Department of Physics, Vancouver BC V6T 1Z1, Canada
[30]University of Alberta, Department of Physics, Edmonton AB T6G 2J1, Canada

[31]Duke University, Dept of Physics, Durham, NC 27708-0305, USA
[32]Research Institute for Particle and Nuclear Physics, H-1525 Budapest, P O Box 49, Hungary
[33]Institute of Nuclear Research, H-4001 Debrecen, P O Box 51, Hungary
[34]Ludwigs-Maximilians-Universität München, Sektion Physik, Am Coulombwall 1, D-85748 Garching, Germany

[a] and at TRIUMF, Vancouver, Canada V6T 2A3
[b] and Royal Society University Research Fellow
[c] and Institute of Nuclear Research, Debrecen, Hungary
[d] and Department of Experimental Physics, Lajos Kossuth University, Debrecen, Hungary
[e] on leave of absence from the University of Freiburg

1 Introduction

The LEP accelerator has provided e^+e^- collisions at ever increasing energies over the past two years. In this paper we present measurements of cross-sections for hadronic, $b\overline{b}$ and lepton pair final states at a centre-of-mass energy $\sqrt{s}$ of 183 GeV; forward-backward asymmetries for the leptonic states are also given. The data were collected by the OPAL detector at LEP in 1997. During 1997 LEP briefly returned to centre-of-mass energies of 130 and 136 GeV, providing an integrated luminosity at these energies similar to the 1995 'LEP1.5' run. We also present cross-sections and asymmetry measurements from these data, and combine them with the results from the earlier run [1].

The analyses presented here are essentially the same as those already presented at lower energies [1]. We use identical techniques to measure s', the square of the centre-of-mass energy of the e^+e^- system after initial-state radiation, and to separate 'non-radiative' events, which have little initial-state radiation, from 'radiative return' to the Z peak. However, we have changed the definition of non-radiative events compared with [1], loosening the requirement from $s'/s > 0.8$ to $s'/s > 0.7225$. This new definition reduces the total measurement errors at the highest centre-of-mass energies, and is the recommended definition of the LEP Electroweak Working Group. Inclusive measurements are corrected to $s'/s > 0.01$ as before. As in our previous publication, we correct our measurements of hadronic, $\mu^+\mu^-$ and $\tau^+\tau^-$ events for the effect of interference between initial- and final-state radiation. We use the same treatment as before of the four-fermion contribution to the two-fermion final states. Because of ambiguities arising from the t-channel contribution, for the e^+e^- final state the acceptance is defined in terms of the angle θ of the electron or positron with respect to the electron beam direction and the acollinearity angle $\theta_{\rm acol}$ between the electron and positron. Cross-sections and asymmetries for e^+e^- are not corrected for interference between initial- and final-state radiation; they are compared to theoretical predictions which include interference.

Measurements of fermion-pair production up to 172 GeV have shown very good agreement with Standard Model expectations [1, 2]. Here we repeat our measurement of the electromagnetic coupling constant $\alpha_{\rm em}(\sqrt{s})$ including the higher energy data. Including data at 183 GeV also allows us to extend the searches for new physics presented in [1]. In particular we obtain improved limits on the energy scale of a possible four-fermion contact interaction. We also present improved limits on the coupling of a heavy particle such as a leptoquark, or a scalar quark (squark) in supersymmetric theories with R-parity violation, which might affect the hadronic cross-section via a t-channel exchange diagram. These analyses are updates of those already presented in [1]. In this paper we extend our search for heavy particles to include those coupling to leptons only. Such particles could be scalar neutrinos (sneutrinos) in supersymmetric theories with R-parity violation. Searches for such particles have been presented in [3]. In this paper we introduce a new technique in which a scan over the complete s' distribution improves our sensitivity for masses between the centre-of-mass energy points of LEP for processes involving s-channel sneutrinos.

The paper is organized as follows. In section 2 we describe the data analysis, cross-section and asymmetry measurements. As the analyses are essentially the same as in [1] we give only a brief description of any changes. In section 3 we compare our measurements to the predictions of the Standard Model and use them to measure the energy dependence of $\alpha_{\rm em}$. The results of searches for new physics are presented in section 4.

2 Data Analysis

The OPAL detector[1], trigger and data acquisition system are fully described elsewhere [4–8]. The analyses presented in this paper use 54–57 pb^{-1} of data collected at centre-of-mass energies of 181–184 GeV during 1997; the actual amount of data varies from channel to channel. The luminosity-weighted mean centre-of-mass energy is 182.69±0.06 GeV [9]. In addition, we present results for about 2.6 (3.3) pb^{-1} of data at 130.00±0.03 (135.98±0.03) GeV collected during 1997 and combine these with earlier results at similar centre-of-mass energies [1].

Selection efficiencies and backgrounds were calculated using Monte Carlo simulations. The set of generators used is identical to that in [1]. At 183 GeV a new background arises from the production of Z-pair events; these were simulated with the grc4f [10] and PYTHIA [11] generators. All events were passed through a simulation [12] of the OPAL detector and processed as for real data.

The luminosity was measured using small-angle Bhabha scattering events recorded in the silicon-tungsten luminometer [1,6]. The overall error on the luminosity measurement amounts to 0.43% at 183 GeV, arising mainly from data statistics (0.26%) and knowledge of the theoretical cross-section (0.25%). At 130 (136) GeV the total error of 1.0% (1.0%) arises mainly from data statistics. Errors from the luminosity measurement are included in all the systematic errors on cross-sections quoted in this paper, and correlations between measurements arising from the luminosity determination are included in all fits.

2.1 Measurements at $\sqrt{s} = 183$ GeV

Hadronic, $\mathrm{e^+e^-}$, $\mu^+\mu^-$ and $\tau^+\tau^-$ events were selected using the criteria described in [1] with some modifications to improve efficiency and background at the higher centre-of-mass energy. Here we briefly describe these changes.

- In the selection of $\mathrm{q\overline{q}}$ events we have rejected events identified as W-pairs according to the criteria of [13], instead of subtracting their expected contribution, resulting in a reduction of about 15% in the overall error on the non-radiative cross-section.
- The background in the muon pair sample has been reduced from 11.5% to 4.7% for inclusive events, from 6.7% to 2.0% for non-radiative events, by introducing a cut on the invariant mass of the muon pair. For inclusive events, if the ratio of the visible energy[2] to the centre-of-mass energy is less than $0.5(m_{\mathrm{Z}}^2/s) + 0.75$ the muon pair invariant mass is required to be greater than 70 GeV. For non-radiative events the mass is required to be greater than $\sqrt{(m_{\mathrm{Z}}^2 + 0.1s)}$ (about 108 GeV).
- The efficiency for tau pairs, particularly radiative events, has been increased by extending the angular acceptance and adjusting cuts so that additional background is suppressed. The result of the changes is to increase the efficiency for inclusive events from 31% to 40%, with a modest (2%) increase in background. In detail the changes are:

[1]OPAL uses a right-handed coordinate system in which the z axis is along the electron beam direction and the x axis is horizontal. The polar angle θ is measured with respect to the z axis and the azimuthal angle ϕ with respect to the x axis.

[2]The visible energy is defined as the scalar sum of the momenta of the two muons plus the energy of the highest energy cluster in the electromagnetic calorimeter [1].

– The acceptance has been increased by requiring that the value of $|\cos\theta|$ for both tau leptons satisfies $|\cos\theta| < 0.9$, instead of demanding that the average value satisfy $|\cos\theta_{\rm av}| < 0.85$.

– The cuts on the total energy of an event have been modified: as before, the total visible energy in the event, derived from the scalar sum of all track momenta plus electromagnetic calorimeter energy, was required to be less than $1.1\sqrt{s}$, but the lower cut on this variable was removed. Instead, the total electromagnetic calorimeter energy was required to be greater than $0.02\sqrt{s}$ and either the total electromagnetic calorimeter energy or the scalar sum of track momenta was required to be greater than $0.2\sqrt{s}$.

– The cuts on the missing momentum and its direction, calculated using electromagnetic calorimeter clusters, have been modified: the missing momentum in the plane transverse to the beam axis was required to exceed $0.015\sqrt{s}$, and the polar angle of the missing momentum was required to satisfy $|\cos\theta| < 0.99$. The cut on the polar angle of the missing momentum calculated using central detector tracks was removed.

– The above modifications increase the efficiency substantially, but also increase the background, particularly from Bhabha events. To reduce this background two new cuts have been introduced. Using the values of θ measured for the two tau leptons (as defined in [1]), the expected energy of each lepton is calculated assuming that the final state consists only of two leptons plus a single unobserved photon along the beam direction. We then require that

$$0.02 < \sqrt{(X_{E1}^2 + X_{E2}^2)} < 0.8,$$

and

$$\sqrt{(X_{P1}^2 + X_{P2}^2)} < 0.8,$$

where $X_{E1,E2}$ are the total electromagnetic calorimeter energies in each tau cone normalized to the expected value calculated above, and $X_{P1,P2}$ are the scalar sums of track momenta in the two tau cones, also normalized to the expected values. These cuts are designed to remove both electron and muon pairs.

In [1] non-radiative events were selected by demanding $s'/s > 0.8$; here we select non-radiative samples by demanding $s'/s > 0.7225$. Distributions of $\sqrt{s'}$ for each channel, determined using kinematic fits for hadrons and track angles for the lepton pairs as in [1], are shown in Fig. 1. Efficiencies, backgrounds and feedthrough of events from lower s' into the non-radiative samples were calculated from Monte Carlo simulation, and are given in Table 1. Efficiencies determined from two-fermion Monte Carlo events have been corrected for the effect of the four-fermion contribution as described in [1]. The numbers of selected events and the measured cross-sections are presented in Table 2, and the cross-sections shown in Fig. 2. As well as cross-sections for $\mathrm{q\overline{q}}$ events, we also present a fully inclusive hadronic cross-section $\sigma(\mathrm{q\overline{q}X})$. This uses the same event selection as is used for $\mathrm{q\overline{q}}$ events but W-pairs are not rejected. The cross-section therefore includes W-pair production with at least one W decaying hadronically. All cross-sections except those for $\mathrm{e^+e^-}$ have been corrected for the contribution of interference between initial- and final-state radiation as described in [1]. The corrections are shown in Table 3.

Efficiencies and backgrounds at $\sqrt{s} = 183$ GeV				
Channel		Efficiency (%)	Background (pb)	Feedthrough (pb)
$q\overline{q}X$		91.0±1.2	4.5±1.0	–
$q\overline{q}$	$s'/s > 0.01$	88.6±1.3	6.4±1.0	–
	$s'/s > 0.7225$	89.9±0.9	2.09±0.09	1.2±0.2
e^+e^-	$\lvert\cos\theta\rvert < 0.9$, $\theta_{\rm acol} < 170°$	98.1±1.1	1.6±0.1	–
	$\lvert\cos\theta_{e^-}\rvert < 0.7$, $\theta_{\rm acol} < 10°$	99.1±0.6	0.26±0.05	–
	$\lvert\cos\theta\rvert < 0.96$, $\theta_{\rm acol} < 10°$	98.9±1.0	10.9±1.1	–
$\mu^+\mu^-$	$s'/s > 0.01$	74.2±0.8	0.31±0.08	–
	$s'/s > 0.7225$	88.3±0.9	0.06±0.02	0.065±0.002
$\tau^+\tau^-$	$s'/s > 0.01$	40.4±0.9	0.61±0.11	–
	$s'/s > 0.7225$	58.9±1.3	0.22±0.04	0.085±0.003

Table 1: Efficiency of selection cuts, background and feedthrough of events with lower s' into the non-radiative samples for each channel at 183 GeV. The errors include Monte Carlo statistics and systematic effects. In the case of electron pairs, the efficiencies are effective values including the efficiency of selection cuts for events within the acceptance region and the effect of acceptance corrections. Values for $b\overline{b}$ production are given in the text.

Cross-sections at $\sqrt{s} = 183$ GeV					
Channel		$\int \mathcal{L}dt$ (pb^{-1})	Events	σ (pb)	$\sigma^{\rm SM}$ (pb)
$q\overline{q}X$		56.9	6373	118.3±1.5±1.6	121.3
$q\overline{q}$	$s'/s > 0.01$	56.9	5598	103.8±1.5±1.7	106.7
	$s'/s > 0.7225$	57.8	1408	23.7±0.7±0.4	24.3
$b\overline{b}$	$s'/s > 0.7225$	55.5	348 – 102	4.6 ±0.6±0.3	3.96
e^+e^-	$\lvert\cos\theta\rvert < 0.9$, $\theta_{\rm acol} < 170°$	57.8	6980	121.4±1.5±1.5	120.0
	$\lvert\cos\theta_{e^-}\rvert < 0.7$, $\theta_{\rm acol} < 10°$		1260	21.7±0.6±0.2	21.8
	$\lvert\cos\theta\rvert < 0.96$, $\theta_{\rm acol} < 10°$		19641	333±3±4	333
$\mu^+\mu^-$	$s'/s > 0.01$	53.9	366	8.70±0.46±0.19	8.31
	$s'/s > 0.7225$		174	3.46±0.26±0.12	3.45
$\tau^+\tau^-$	$s'/s > 0.01$	53.9	216	8.38±0.57±0.34	8.30
	$s'/s > 0.7225$		123	3.31±0.30±0.11	3.45

Table 2: Integrated luminosity used in the analysis, numbers of selected events and measured cross-sections at $\sqrt{s}$=182.69 GeV. In the $b\overline{b}$ case the numbers of forward and backward tags are given. For the cross-sections, the first error shown is statistical, the second systematic. As in [1], the cross-sections for hadrons, $b\overline{b}$, $\mu^+\mu^-$ and $\tau^+\tau^-$ are defined to cover phase-space up to the limit imposed by the s'/s cut, with $\sqrt{s'}$ defined as the invariant mass of the outgoing two-fermion system *before* final-state photon radiation. The contribution of interference between initial- and final-state radiation has been removed. The last column shows the Standard Model cross-section predictions from ZFITTER [14] (hadrons, $b\overline{b}$, $\mu^+\mu^-$, $\tau^+\tau^-$) and ALIBABA [15] (e^+e^-).

Interference Corrections			
$s'/s > 0.01$	130.12 GeV	136.08 GeV	182.69 GeV
$\Delta\sigma/\sigma_{\rm SM}$(had) (%)	$+0.10 \pm 0.00 \pm 0.10$	$+0.10 \pm 0.00 \pm 0.10$	$+0.14 \pm 0.00 \pm 0.14$
$\Delta\sigma/\sigma_{\rm SM}(\mu\mu)$ (%)	-0.35 ± 0.05	-0.33 ± 0.03	-0.43 ± 0.04
$\Delta\sigma/\sigma_{\rm SM}(\tau\tau)$ (%)	-0.44 ± 0.09	-0.40 ± 0.07	-0.46 ± 0.06
$\Delta A_{\rm FB}(\mu\mu)$	-0.0040 ± 0.0006	-0.0029 ± 0.0003	-0.0052 ± 0.0007
$\Delta A_{\rm FB}(\tau\tau)$	-0.0055 ± 0.0014	-0.0056 ± 0.0013	-0.0055 ± 0.0009
$\Delta A_{\rm FB}$(combined)	-0.0046 ± 0.0008	-0.0036 ± 0.0006	-0.0055 ± 0.0008
$s'/s > 0.7225$	130.12 GeV	136.08 GeV	182.69 GeV
$\Delta\sigma/\sigma_{\rm SM}$(had) (%)	$+0.8 \pm 0.2 \pm 0.4$	$+0.9 \pm 0.3 \pm 0.4$	$+1.2 \pm 0.3 \pm 0.6$
$\Delta\sigma/\sigma_{\rm SM}(\mu\mu)$ (%)	-1.4 ± 0.4	-1.4 ± 0.4	-1.4 ± 0.4
$\Delta\sigma/\sigma_{\rm SM}(\tau\tau)$ (%)	-1.2 ± 0.4	-1.1 ± 0.3	-1.2 ± 0.3
$\Delta A_{\rm FB}(\mu\mu)$	-0.015 ± 0.004	-0.007 ± 0.002	-0.015 ± 0.004
$\Delta A_{\rm FB}(\tau\tau)$	-0.011 ± 0.004	-0.008 ± 0.002	-0.012 ± 0.004
$\Delta A_{\rm FB}$(combined)	-0.014 ± 0.004	-0.007 ± 0.002	-0.014 ± 0.004
$s'/s > 0.7225$	133.29 GeV		182.69 GeV
$\Delta\sigma/\sigma_{\rm SM}(\mathrm{b\overline{b}})$ (%)	$-1.0 \pm 0.3 \pm 0.4$		$-1.4 \pm 0.4 \pm 0.6$
$\Delta R_{\rm b}/R_{\rm b,SM}$ (%)	$-1.7 \pm 0.5 \pm 0.6$		$-2.3 \pm 0.6 \pm 1.1$

Table 3: Corrections $\Delta\sigma$ and $\Delta A_{\rm FB}$ which have been applied to the measured cross-sections and asymmetries in order to remove the contribution from interference between initial- and final-state radiation. Cross-section corrections are expressed as a fraction of the expected Standard Model cross-section, while asymmetry corrections are given as absolute numbers, and depend on the observed asymmetry. The first error reflects the uncertainty from modelling the selection efficiency for the interference cross-section, and is very small for hadrons because the efficiency is large and depends only weakly on $\cos\theta$. The second error is our estimate of possible additional QCD corrections for the hadrons [1].

Systematic errors on these measurements are generally similar to those at 172 GeV. In the case of inclusive hadrons they are dominated by uncertainties in the selection efficiency (1.2%) and background from two-photon events (1.0%), whereas the main uncertainties for non-radiative hadronic events arise from their separation from radiative events (1.1%) and knowledge of the efficiency (1.1%). As a cross-check, we have calculated the hadron cross-sections without rejecting W-pair events, by subtracting their expected contribution instead. The measured values of 103.9±1.6±1.6 pb ($s'/s > 0.01$) and 23.7±0.8±0.5 pb ($s'/s > 0.7225$), after correction for interference between initial- and final-state radiation, are in good agreement with the values in Table 2. The main systematic errors on the electron pair cross-sections arise from uncertainties in the matching of central detector tracks to electromagnetic calorimeter clusters, and knowledge of the acceptance correction and modelling of the edge of the acceptance. Those on the muon and tau pair cross-sections arise mainly from uncertainties in background and efficiency, and are substantially smaller than the statistical errors.

Measurements of the forward-backward asymmetry for lepton pairs are given in Table 4 and compared with lower energy measurements in Fig. 3. As before [1], only events where the charge can be reliably determined are used for the asymmetry measurements. The final values for muon and tau pairs are obtained by averaging the results measured using the negative par-

ticle with those obtained using the positive particle to reduce systematic effects. Muon and tau asymmetries are corrected to the full angular range by applying a multiplicative correction obtained from ZFITTER to the asymmetry measured within the acceptance of the selection cuts. As at lower energies, the dominant errors on the asymmetry measurements are statistical, with systematic effects from the correction for interference between initial- and final-state radiation, charge misassignment and θ measurement amounting to 0.01 or less in all cases. The corrected angular distributions for the lepton pairs are given in Table 5. The angular distribution of the primary quark in non-radiative hadronic events is given in Table 6. The angular distributions are plotted in Fig. 4.

Asymmetries at $\sqrt{s} = 183$ GeV					
		N_{F}	N_{B}	A_{FB}	$A_{\mathrm{FB}}^{\mathrm{SM}}$
$\mathrm{e^+e^-}$	$\lvert\cos\theta_{\mathrm{e^-}}\rvert < 0.7$ and $\theta_{\mathrm{acol}} < 10^\circ$	1088	140	0.776±0.019	0.813
$\mu^+\mu^-$	$s'/s > 0.01$	229	122	0.26±0.05	0.28
	$s'/s > 0.7225$	127.5	38.5	0.54±0.07	0.57
$\tau^+\tau^-$	$s'/s > 0.01$	149	58	0.39±0.08	0.28
	$s'/s > 0.7225$	97	23	0.68±0.09	0.57
Combined	$s'/s > 0.01$			0.31±0.04	0.28
$\mu^+\mu^-$ and $\tau^+\tau^-$	$s'/s > 0.7225$			0.60±0.05	0.57

Table 4: The numbers of forward (N_{F}) and backward (N_{B}) events and measured asymmetry values at 182.69 GeV. The measured asymmetry values include corrections for background and efficiency, and in the case of muons and taus are corrected to the full solid angle. The errors shown are the combined statistical and systematic errors. The asymmetries for $\mu^+\mu^-$, $\tau^+\tau^-$ and for the combined $\mu^+\mu^-$ and $\tau^+\tau^-$ are shown after the correction for interference between initial- and final-state radiation. The final column shows the Standard Model predictions of ALIBABA for $\mathrm{e^+e^-}$ and ZFITTER for the other final states.

We have measured R_{b}, the ratio of the cross-section for $\mathrm{b\overline{b}}$ production to the hadronic cross-section, for $s'/s > 0.7225$. As in [1], $\mathrm{b\overline{b}}$ events were tagged by reconstructing secondary vertices in the plane transverse to the beam direction, and a 'folded tag' technique was used. In this method R_{b} is determined from the difference between the number of events with $L/\sigma_L > 3$ (forward tags) and the number with $L/\sigma_L < -3$ (backward tags), where L is the signed decay length measured from the primary vertex to the secondary vertex and σ_L is the error on this length. The net efficiencies, i.e. differences between forward and backward tagging efficiencies, determined from Monte Carlo, were 0.398±0.021, 0.095±0.004 and 0.0105±0.0024 for b, c and light quarks respectively, similar to the values at 172 GeV. The systematic errors on R_{b} are again dominated by modelling of b and c fragmentation and decay, estimated using the prescription in [19], and track parameter resolution.

This measurement used hadronic events with $s'/s > 0.7225$, selected as for the cross-section measurement. W-pair events were rejected as described above. A new background arises at 183 GeV from Z-pair production; the probability of a Z-pair event being tagged was estimated to be (33.5±1.0)%, and the expected contribution from these was subtracted; this contribution is small, amounting to only 1.6% of the tagged sample. After background subtraction the b purity of the tagged $\mathrm{q\overline{q}}$ sample was estimated to be 68%.

e^+e^-			
$[\cos\theta_{\min}, \cos\theta_{\max}]$	$d\sigma/d\cos\theta$ (pb)		
	130.12 GeV	136.08 GeV	182.69 GeV
$[-0.9, -0.7]$	$4\pm^{3}_{2}$	$5\pm^{3}_{2}$	$1.2\pm^{0.4}_{0.3}$
$[-0.7, -0.5]$	$4\pm^{3}_{2}$	$4\pm^{3}_{2}$	2.1 ± 0.4
$[-0.5, -0.3]$	$6\pm^{3}_{2}$	$8\pm^{4}_{3}$	2.3 ± 0.5
$[-0.3, -0.1]$	$6\pm^{4}_{2}$	$9\pm^{4}_{3}$	4.8 ± 0.7
$[-0.1, \ 0.1]$	$13\pm^{5}_{4}$	$8\pm^{4}_{3}$	6.1 ± 0.7
$[\ 0.1, \ 0.3]$	23 ± 5	18 ± 4	9.5 ± 0.9
$[\ 0.3, \ 0.5]$	45 ± 7	35 ± 6	21.1 ± 1.4
$[\ 0.5, \ 0.7]$	113 ± 11	122 ± 10	62 ± 2
$[\ 0.7, \ 0.9]$	839 ± 30	725 ± 27	458 ± 8
$\mu^+\mu^-$			
$[\cos\theta_{\min}, \cos\theta_{\max}]$	$d\sigma/d\cos\theta$ (pb)		
	130.12 GeV	136.08 GeV	182.69 GeV
$[-1.0, -0.8]$	$0\pm^{3}_{1}$	$-1\pm^{1}_{0}$	$0.4\pm^{0.4}_{0.2}$
$[-0.8, -0.6]$	$3\pm^{3}_{2}$	$2\pm^{3}_{1}$	$0.7\pm^{0.4}_{0.3}$
$[-0.6, -0.4]$	$0\pm^{2}_{1}$	$0\pm^{2}_{1}$	$0.5\pm^{0.4}_{0.2}$
$[-0.4, -0.2]$	$6\pm^{4}_{3}$	$5\pm^{3}_{2}$	$0.9\pm^{0.4}_{0.3}$
$[-0.2, \ 0.0]$	$3\pm^{3}_{2}$	$1\pm^{2}_{1}$	$1.2\pm^{0.5}_{0.3}$
$[\ 0.0, \ 0.2]$	$2\pm^{3}_{2}$	$3\pm^{3}_{2}$	1.8 ± 0.4
$[\ 0.2, \ 0.4]$	$6\pm^{4}_{3}$	$6\pm^{3}_{2}$	2.4 ± 0.5
$[\ 0.4, \ 0.6]$	$5\pm^{4}_{2}$	$10\pm^{4}_{3}$	1.9 ± 0.5
$[\ 0.6, \ 0.8]$	$5\pm^{4}_{3}$	$9\pm^{4}_{3}$	2.5 ± 0.5
$[\ 0.8, \ 1.0]$	$9\pm^{5}_{4}$	$18\pm^{7}_{5}$	4.7 ± 0.9
$\tau^+\tau^-$			
$[\cos\theta_{\min}, \cos\theta_{\max}]$	$d\sigma/d\cos\theta$ (pb)		
	130.12 GeV	136.08 GeV	182.69 GeV
$[-1.0, -0.8]$	$-1\pm^{10}_{0}$	$-1\pm^{9}_{0}$	$0.7\pm^{0.9}_{0.5}$
$[-0.8, -0.6]$	$0\pm^{1}_{0}$	$0\pm^{1}_{0}$	$0.0\pm^{0.3}_{0.1}$
$[-0.6, -0.4]$	$-1\pm^{2}_{0}$	$2\pm^{3}_{2}$	$0.0\pm^{0.3}_{0.1}$
$[-0.4, -0.2]$	$2\pm^{4}_{2}$	$0\pm^{1}_{0}$	$0.7\pm^{0.5}_{0.3}$
$[-0.2, \ 0.0]$	$3\pm^{4}_{2}$	$1\pm^{3}_{1}$	$1.5\pm^{0.6}_{0.5}$
$[\ 0.0, \ 0.2]$	$2\pm^{4}_{2}$	$4\pm^{3}_{2}$	$1.6\pm^{0.6}_{0.5}$
$[\ 0.2, \ 0.4]$	$1\pm^{4}_{2}$	$4\pm^{4}_{2}$	$1.5\pm^{0.6}_{0.5}$
$[\ 0.4, \ 0.6]$	$7\pm^{5}_{3}$	$7\pm^{4}_{3}$	2.5 ± 0.6
$[\ 0.6, \ 0.8]$	$7\pm^{5}_{3}$	$8\pm^{5}_{3}$	4.3 ± 0.8
$[\ 0.8, \ 1.0]$	$14\pm^{19}_{11}$	$7\pm^{15}_{7}$	$3.9\pm^{1.6}_{1.3}$

Table 5: Differential cross-sections for lepton pair production. The values for e^+e^- are for $\theta_{\rm acol} < 10^\circ$; those for $\mu^+\mu^-$ and $\tau^+\tau^-$ are for $s'/s > 0.7225$ and are corrected to no interference between initial- and final-state radiation. The values for 130 and 136 GeV are from the combined 1995 and 1997 data. Negative values arise when fewer events are observed than expected from background. Errors include statistical and systematic effects combined, with the former dominant.

Hadrons			
$\lvert\cos\theta\rvert$	$\mathrm{d}\sigma/\mathrm{d}\lvert\cos\theta\rvert$ (pb)		
	130.12 GeV	136.08 GeV	182.69 GeV
$[0.0, 0.1]$	70±12	48±9	17.0±1.8
$[0.1, 0.2]$	52±9	64±10	17.6±1.8
$[0.2, 0.3]$	70±11	56±10	17.7±1.9
$[0.3, 0.4]$	70±11	63±10	19.9±2.0
$[0.4, 0.5]$	64±10	44±9	23.1±2.1
$[0.5, 0.6]$	79±12	39±8	24.6±2.2
$[0.6, 0.7]$	81±12	78±11	27.2±2.3
$[0.7, 0.8]$	94±13	81±11	26.1±2.2
$[0.8, 0.9]$	85±12	82±11	31.2±2.4
$[0.9, 1.0]$	160±23	123±19	32.0±3.2

Table 6: Differential cross-sections for $\mathrm{q\overline{q}}$ production, for $s'/s > 0.7225$. The values are corrected to no interference between initial- and final-state radiation as in [1]. Errors include statistical and systematic effects combined, with the former dominant.

We obtain a value of R_b, after correcting for interference between initial- and final-state radiation, of

$$R_\mathrm{b}(\sqrt{s} = 182.69 \text{ GeV}) = 0.195 \pm 0.023 \pm 0.013,$$

where the first error is statistical and the second systematic; the value of the $\mathrm{b\overline{b}}$ cross-section derived from the measurement of the hadronic cross-section and R_b is given in Table 2.

2.2 Measurements at $\sqrt{s} = 130$–136 GeV

The analyses of the 130 and 136 GeV data were unchanged from those described in [1], with the exception of the modification of the s' cut used to define non-radiative events. The numbers of selected events and measured cross-sections are given in Table 7, and the forward-backward asymmetry values for the leptonic channels in Table 8. The values are generally in good agreement with those obtained from the data collected in 1995 at similar centre-of-mass energies [1], after correcting the latter to $s'/s > 0.7225$ in the non-radiative cases. We have combined the measurements from the two sets of data; when measurements of non-radiative hadrons, muons and taus were combined the new s' cut was applied to the 1995 data. The combined results are also shown in Tables 7 and 8. Corrected angular distributions for the lepton pairs are given in Table 5 and for the hadronic events in Table 6.

The measurement of R_b for the 1997 data benefited, in comparison with the 1995 measurement, from the longer silicon microvertex detector installed in 1996, which enabled the cut on the polar angle of the thrust axis to be increased from $\lvert\cos\theta\rvert < 0.8$ to $\lvert\cos\theta\rvert < 0.9$, as for the measurements at 161–183 GeV. For the 1997 combined 130 and 136 GeV data we obtain a value of R_b, after correction for initial-final state interference, of

$$R_\mathrm{b}(\sqrt{s} = 133.38 \text{ GeV}) = 0.201 \pm 0.036 \pm 0.013,$$

where the first error is statistical and the second systematic. Combining with the 1995 measurement [1] and taking account of correlated systematic errors, gives

$$R_{\mathrm{b}}(\sqrt{s} = 133.29 \text{ GeV}) = 0.198 \pm 0.026 \pm 0.013.$$

The corresponding $\mathrm{b\overline{b}}$ cross-sections, calculated from the hadronic cross-sections and the R_{b} measurements, are given in Table 7.

3 Comparison with Standard Model Predictions

The cross-section and asymmetry measurements at 183 GeV are compared with the Standard Model predictions in Tables 2 and 4 respectively. The Standard Model Predictions are calculated using ALIBABA [15] for the $\mathrm{e^+e^-}$ final state and ZFITTER [14] for all other final states; input parameters and flags used in ZFITTER are as in [1]. The agreement is generally good, as is also seen in the case of the 130 and 136 GeV data in Tables 7 and 8. Figure 2 shows cross-sections, for both inclusive and non-radiative events, as a function of $\sqrt{s}$, while Fig. 3 shows the measured asymmetry values. The angular distributions for all channels at 183 GeV are compared with Standard Model predictions in Fig. 4.

In Fig. 5 we show the ratio of measured hadronic cross-sections to theoretical muon pair cross-sections as a function of centre-of-mass energy for two cases. In the first case the numerator of this ratio is the inclusive $\mathrm{q\overline{q}X}$ cross-section, in the second case it is the non-radiative $\mathrm{q\overline{q}}$ cross-section corrected to the Born level. In each case the denominator is the corresponding muon pair cross-section calculated using ZFITTER. The inclusive ratio clearly shows the effect of $\mathrm{W^+W^-}$ production.

3.1 Energy Dependence of α_{em}

In [1] we used non-radiative cross-section and asymmetry measurements to measure the electromagnetic coupling constant α_{em} at LEP2 energies. We have repeated this fit including the new measurements of hadronic, $\mu^+\mu^-$ and $\tau^+\tau^-$ cross-sections, R_{b}, and the combined muon and tau asymmetry values, for $s'/s > 0.7225$, presented here. As before, we form the χ^2 between the measured values and the Standard Model predictions calculated as a function of $\alpha_{\mathrm{em}}(\sqrt{s})$ using ZFITTER, with all other ZFITTER input parameters fixed. Correlations between measurements are fully taken into account.

We have performed separate fits to the 183 GeV measurements and the updated 130–136 GeV measurements; the 130 and 136 GeV measurements are combined for this analysis. The results of these fits are given in Table 9. The inclusion of the new data at 130–136 GeV has not reduced the relative error on the measurement at 133 GeV because the measured cross-sections and asymmetries, particularly the hadronic cross-section, now lie closer to the Standard Model expectation. The sensitivity of the measurements to α_{em} is nonlinear, resulting in smaller errors as the value moves away from the Standard Model expectation. We have also performed a fit to data at all centre-of-mass energies, in which α_{em} runs with energy with a slope corresponding to the fitted value. As input to the combined fit we use the measurements at 183 GeV and the combined data at 130–136 GeV presented here, together with measurements at 161 and 172 GeV from [1]. The result of the combined fit is

$$1/\alpha_{\mathrm{em}}(169.34 \text{ GeV}) = 127.8^{+4.1}_{-3.6},$$

Cross-sections at $\sqrt{s}$ = 130 GeV					
		1997		1995+1997	
		130.00 GeV		130.12 GeV	130.12 GeV
Channel		Events	σ (pb)	σ (pb)	σ^{SM} (pb)
$q\overline{q}$	$s'/s > 0.01$	807	350±13±5	332±8±5	331
	$s'/s > 0.7225$	241	88.5±5.8±1.8	79.7±3.8±1.6	83.1
e^+e^-	$\lvert\cos\theta\rvert < 0.9$, $\theta_{\mathrm{acol}} < 170°$	609	235±10±4	227±7±3	238
	$\lvert\cos\theta_{e^-}\rvert < 0.7$, $\theta_{\mathrm{acol}} < 10°$	113	43.2±4.1±0.6	42.3±2.9±0.5	43.2
	$\lvert\cos\theta\rvert < 0.96$, $\theta_{\mathrm{acol}} < 10°$	1718	647±16±10	631±11±8	647
$\mu^+\mu^-$	$s'/s > 0.01$	40	18.1±2.9±0.7	21.2±2.2±0.5	22.1
	$s'/s > 0.7225$	17	5.5 ±1.4±0.5	7.6 ±1.1±0.3	8.5
$\tau^+\tau^-$	$s'/s > 0.01$	24	22.5±4.6±0.7	25.1±3.4±0.8	22.1
	$s'/s > 0.7225$	11	6.4 ±1.9±0.3	6.8 ±1.4±0.3	8.5
Cross-sections at $\sqrt{s}$ = 136 GeV					
		1997		1995+1997	
		135.98 GeV		136.08 GeV	136.08 GeV
Channel		Events	σ (pb)	σ (pb)	σ^{SM}
$q\overline{q}$	$s'/s > 0.01$	907	277±9±4	271±7±4	275
	$s'/s > 0.7225$	228	65.5±4.4±1.5	66.7±3.3±1.3	66.9
e^+e^-	$\lvert\cos\theta\rvert < 0.9$, $\theta_{\mathrm{acol}} < 170°$	704	209±8 ±3	204±6±3	217
e^+e^-	$\lvert\cos\theta_{e^-}\rvert < 0.7$, $\theta_{\mathrm{acol}} < 10°$	144	42.4±3.6±0.6	40.2±2.6±0.4	39.6
e^+e^-	$\lvert\cos\theta\rvert < 0.96$, $\theta_{\mathrm{acol}} < 10°$	2034	588±13±9	585±10±7	593
$\mu^+\mu^-$	$s'/s > 0.01$	72	25.0±3.0 ±0.6	25.2±2.2±0.5	18.9
	$s'/s > 0.7225$	33	9.5 ±1.7 ±0.4	10.4±1.3±0.3	7.3
$\tau^+\tau^-$	$s'/s > 0.01$	23	16.3±3.4 ±0.6	19.5±2.8±0.6	18.9
	$s'/s > 0.7225$	15	6.9 ±1.8 ±0.2	7.3±1.4±0.3	7.3
Cross-sections at $\sqrt{s}$ = 133 GeV					
		1997		1995+1997	
		133.38 GeV		133.29 GeV	133.29 GeV
Channel		Events	σ (pb)	σ (pb)	σ^{SM}
$b\overline{b}$	$s'/s > 0.7225$	126 – 35	15.2±2.8±1.0	14.4±2.0±1.0	13.5

Table 7: Numbers of selected events and measured cross-sections for the 130 and 136 GeV data taken in 1997. In the $b\overline{b}$ case the 130 and 136 GeV data are combined, and numbers of forward and backward tags are given. The cross-sections obtained by combining these results with the results from data taken at these energies in 1995 [1] are also given, and compared with the Standard Model predictions from ALIBABA for electron pairs and ZFITTER for all other final states. Cross-sections are given after the correction for interference between initial- and final-state radiation; values of these corrections are given in Table 3. The first error is statistical, the second systematic.

Asymmetries at $\sqrt{s} = 130$ GeV						
		1997 130.00 GeV			1995+1997 130.12 GeV	130.12 GeV
		N_F	N_B	A_{FB}	A_{FB}	A_{FB}^{SM}
e^+e^-	$\lvert\cos\theta_{e^-}\rvert < 0.7$ and $\theta_{acol} < 10°$	99	9	0.84 ±0.05	0.81±0.04	0.80
$\mu^+\mu^-$	$s'/s > 0.01$	24.5	15	0.24±0.16	0.24±0.11	0.29
	$s'/s > 0.7225$	11.5	5.5	$0.40^{+0.30}_{-0.41}$	$0.40^{+0.18}_{-0.22}$	0.70
$\tau^+\tau^-$	$s'/s > 0.01$	14	8	0.25±0.23	0.32±0.15	0.29
	$s'/s > 0.7225$	7	3	$0.53^{+0.35}_{-0.57}$	$0.80^{+0.20}_{-0.31}$	0.70
Combined	$s'/s > 0.01$			0.24±0.14	0.26±0.09	0.29
$\mu^+\mu^-$ and $\tau^+\tau^-$	$s'/s > 0.7225$			0.46±0.23	0.55±0.13	0.70
Asymmetries at $\sqrt{s} = 136$ GeV						
		1997 135.98 GeV			1995+1997 136.08 GeV	136.08 GeV
		N_F	N_B	A_{FB}	A_{FB}	A_{FB}^{SM}
e^+e^-	$\lvert\cos\theta_{e^-}\rvert < 0.7$ and $\theta_{acol} < 10°$	129	15	0.79 ±0.05	0.77±0.04	0.80
$\mu^+\mu^-$	$s'/s > 0.01$	40.5	29	0.14±0.12	0.23±0.09	0.29
	$s'/s > 0.7225$	25.5	7	$0.64^{+0.16}_{-0.23}$	$0.71^{+0.11}_{-0.14}$	0.68
$\tau^+\tau^-$	$s'/s > 0.01$	15	7	0.23±0.25	0.33±0.17	0.29
	$s'/s > 0.7225$	11.5	3.5	$0.62^{+0.26}_{-0.41}$	$0.86^{+0.16}_{-0.26}$	0.68
Combined	$s'/s > 0.01$			0.15±0.11	0.25±0.08	0.29
$\mu^+\mu^-$ and $\tau^+\tau^-$	$s'/s > 0.7225$			0.65±0.13	0.76±0.09	0.68

Table 8: The numbers of forward (N_F) and backward (N_B) events and measured asymmetry values for the 130 and 136 GeV data taken in 1997. The values obtained by combining these results with the results from data taken at these energies in 1995 [1] are also given. Measured asymmetry values include corrections for background and efficiency. In the case of muons and taus they are corrected to the full solid angle, and are shown after the correction for interference between initial- and final-state radiation. The errors shown are the combined statistical and systematic errors; in each case the systematic error is 0.01 or less. The final column shows the Standard Model predictions of ALIBABA for e^+e^- and ZFITTER for the other final states.

where the value of $\alpha_{\rm em}$ is quoted at the centre-of-mass energy corresponding to the luminosity-weighted average of $1/s$. The errors on the fitted value of $\alpha_{\rm em}$ arise from the errors on the measurements; errors due to uncertainties in the ZFITTER input parameters are negligible.

The measured values of $\alpha_{\rm em}$ are shown in Fig. 6. They are consistent with the Standard Model expectation. The value of $1/\alpha_{\rm em}$ obtained from the combined measurements is 2.3 standard deviations below the low energy limit of 137.0359979±0.0000032 [25].

The fit described above uses measurements of cross-sections which depend on the measurement of luminosity, which itself assumes the Standard Model running of $\alpha_{\rm em}$ from $(Q^2 = 0)$ to typically $Q^2 = (3.5\ {\rm GeV})^2$, where $1/\alpha_{\rm em} \simeq 134$. Therefore it measures the running of $\alpha_{\rm em}$ only from $Q_{\rm lumi} \simeq 3.5$ GeV onwards. To become independent of this assumption, as in [1] we have repeated the combined fit replacing the cross-sections for hadrons, muon and tau pairs with the ratios $\sigma(\mu\mu)/\sigma(\mathrm{q\overline{q}})$ and $\sigma(\tau\tau)/\sigma(\mathrm{q\overline{q}})$. The result of this fit is $1/\alpha_{\rm em}(169.34\ {\rm GeV}) = 126.8^{+5.0}_{-4.4}$, with a χ^2 of 8.7 for 15 degrees of freedom. The value is close to that obtained from the cross-section fit but with somewhat larger errors. The difference in χ^2 between the best fit and the assumption that $\alpha_{\rm em}$ does not run with energy but is fixed at the low energy limit is $(1.91)^2$. If $\alpha_{\rm em}$ did not run with energy, the probability of measuring $1/\alpha_{\rm em}$ lower than 137.0359979 by this amount would be 2.8%, thus demonstrating the running of $\alpha_{\rm em}$ from $(Q^2 = 0)$ to LEP2 energies. This measurement of $\alpha_{\rm em}$ is independent of low-mass hadronic loops and nearly independent of the mass of the Higgs boson and $\alpha_{\rm s}$; it can be scaled to the mass of the Z, giving $1/\alpha_{\rm em}(91.19\ {\rm GeV}) = 127.8^{+4.5}_{-3.9}$.

	Fit		Standard Model	
$\sqrt{s}$ (GeV)	$1/\alpha_{\rm em}$	χ^2/d.o.f.	$1/\alpha_{\rm em}$	χ^2/d.o.f.
133.29	$125.1^{+8.1}_{-6.4}$	2.2/4	128.3	2.4/5
182.69	$131.2^{+6.5}_{-5.3}$	2.2/4	127.9	2.6/5
169.34	$127.8^{+4.1}_{-3.6}$	11.7/19	128.0	11.7/20

Table 9: Results of fits for $\alpha_{\rm em}$. The first two rows show the fits to data at each centre-of-mass energy, the last row the combined fit to these energies and measurements at 161 and 172 GeV [1]. The Standard Model values of $1/\alpha_{\rm em}$, and the χ^2 between the measurements and the Standard Model predictions are also given for comparison.

4 Constraints on New Physics

New physics would be revealed by deviations of the measured data from Standard Model predictions. The good agreement between data and the Standard Model places severe constraints on the energy scale of new phenomena, which are investigated in this section.

For effects arising from the exchange of a new particle with mass $m_{\rm X}$ the contact interaction offers an appropriate framework for $m_{\rm X} \gg \sqrt{s}$. Limits on the energy scale Λ are presented for various models. For lower mass ranges, $\sqrt{s} \lesssim m_{\rm X} < \Lambda$, propagator and width effects must be taken into account. The results of a search for heavy particles which couple to leptons, or to both quarks and leptons, are reported. A new technique has been developed in which a scan over the complete s' distribution significantly improves our sensitivity to the s-channel process mediated by particles such as R-parity violating sneutrinos.

4.1 Limits on Four-fermion Contact Interactions

A very general framework in which to search for the effect of new physics is the four-fermion contact interaction. In this framework [26] the Standard Model Lagrangian for $e^+e^- \to f\overline{f}$ is extended by a term describing a new effective interaction with an unknown coupling constant g and an energy scale Λ:

$$\mathcal{L}^{\text{contact}} = \frac{g^2}{(1+\delta)\Lambda^2} \sum_{i,j=\text{L,R}} \eta_{ij} [\bar{e}_i \gamma^\mu e_i][\bar{f}_j \gamma_\mu f_j], \quad (1)$$

where $\delta = 1$ for $e^+e^- \to e^+e^-$ and $\delta = 0$ otherwise. Here $e_L(f_L)$ and $e_R(f_R)$ are chirality projections of electron (fermion) spinors, and η_{ij} describes the chiral structure of the interaction. The parameters η_{ij} are free in these models, but typical values are between -1 and $+1$, depending on the type of theory assumed [27]. Here we consider the same set of models as in [1].

We have repeated the analysis described in [1], including the measurements of the angular distributions for the non-radiative $e^+e^- \to e^+e^-$, $e^+e^- \to \mu^+\mu^-$, $e^+e^- \to \tau^+\tau^-$ processes, the non-radiative cross-section for $e^+e^- \to q\overline{q}$, and the measurement of R_b at 183 GeV presented here. We have also replaced the measurements at 130–136 GeV used in [1] with the values from the combined 1995+1997 data presented here. As before, we use a maximum likelihood fit in the case of the lepton angular distributions, and a χ^2 fit for the hadronic and $b\overline{b}$ cross-sections. Radiative corrections to the lowest order cross-section are taken into account as described in [1]. Limits on the energy scale Λ are extracted assuming $g^2/4\pi = 1$.

The results are shown in Table 10 and illustrated graphically in Fig. 7; the notation for the different models is identical to [1,28]. The values for $b\overline{b}$ are obtained by fitting the cross-sections for $b\overline{b}$ production, and there is no requirement on whether or not the new interaction couples to other flavours. By contrast, those for up-type quarks and down-type quarks are obtained by fitting the hadronic cross-sections assuming the new interaction couples only to one flavour. The two sets of values Λ_+ and Λ_- shown in Table 10 correspond to positive and negative values of $\varepsilon = 1/\Lambda^2$ respectively, reflecting the two possible signs of η_{ij} in equation (1). As before, the data are particularly sensitive to the VV and AA models; the combined data give limits on Λ in the range 8–10 TeV for these models, roughly 2 TeV higher than those for 130–172 GeV data alone. For the other models the limits generally lie in the range 5–8 TeV, approximately 1.5 TeV above those from previous data. Those for the $\overline{\mathcal{O}}_{\text{DB}}$ model [29] are larger (14–15 TeV) because the values of the η parameters are larger for this model.

4.2 Limits on Heavy Particles

In this section we present the results of a search under the explicit assumption that the new phenomena are due to a heavy particle which couples to leptons, or to quarks and leptons. The sensitivity of the OPAL data to these phenomena is tested separately for the hadronic and leptonic events. Although we use specific particles in the analyses presented below, the results are generally applicable for any heavy particle with similar properties.

4.2.1 Particles Coupling to Quarks and Leptons

Examples of new heavy particles which could contribute to the hadronic cross-section are leptoquarks [30] or squarks in supersymmetric theories with R-parity violation [31]. Beyond the

Channel		LL $[\pm1,0,0,0]$	RR $[0,\pm1,0,0]$	LR $[0,0,\pm1,0]$	RL $[0,0,0,\pm1]$	VV $[\pm1,\pm1,\pm1,\pm1]$	AA $[\pm1,\pm1,\mp1,\mp1]$	LL+RR $[\pm1,\pm1,0,0]$	LR+RL $[0,0,\pm1,\pm1]$	$\overline{\mathcal{O}}_{\mathrm{DB}}$ $[\pm1,\pm4,\pm2,\pm2]$
e^+e^-	ε_0	$0.009^{+0.044}_{-0.042}$	$0.009^{+0.045}_{-0.043}$	$0.006^{+0.024}_{-0.021}$	$0.006^{+0.024}_{-0.021}$	$0.003^{+0.008}_{-0.008}$	$-0.003^{+0.013}_{-0.015}$	$0.004^{+0.021}_{-0.022}$	$0.003^{+0.011}_{-0.011}$	$0.001^{+0.004}_{-0.004}$
	Λ_+	3.1	3.1	4.3	4.3	7.4	6.7	4.6	6.2	10.8
	Λ_-	3.8	3.8	5.3	5.3	8.5	5.5	5.2	7.3	12.4
$\mu^+\mu^-$	ε_0	$-0.001^{+0.026}_{-0.027}$	$-0.003^{+0.029}_{-0.030}$	$0.013^{+0.034}_{-0.037}$	$0.013^{+0.034}_{-0.037}$	$0.002^{+0.010}_{-0.010}$	$-0.004^{+0.013}_{-0.012}$	$-0.001^{+0.014}_{-0.014}$	$0.007^{+0.018}_{-0.019}$	$0.001^{+0.005}_{-0.005}$
	Λ_+	4.5	4.3	3.6	3.6	6.8	6.9	6.1	4.9	10.3
	Λ_-	4.3	4.0	1.7	1.7	7.4	5.9	6.0	5.7	11.0
$\tau^+\tau^-$	ε_0	$0.005^{+0.032}_{-0.035}$	$0.006^{+0.036}_{-0.038}$	$-0.111^{+0.078}_{-0.103}$	$-0.111^{+0.078}_{-0.103}$	$-0.009^{+0.013}_{-0.013}$	$0.018^{+0.017}_{-0.016}$	$0.002^{+0.018}_{-0.017}$	$-0.048^{+0.030}_{-0.036}$	$-0.004^{+0.006}_{-0.006}$
	Λ_+	3.8	3.7	4.7	4.7	7.4	4.4	5.2	6.3	10.8
	Λ_-	4.0	3.8	1.9	1.9	5.3	7.3	5.6	2.0	8.1
$\ell^+\ell^-$	ε_0	$0.001^{+0.018}_{-0.019}$	$0.001^{+0.020}_{-0.020}$	$-0.003^{+0.018}_{-0.017}$	$-0.003^{+0.018}_{-0.017}$	$0.000^{+0.006}_{-0.006}$	$0.001^{+0.008}_{-0.008}$	$0.000^{+0.010}_{-0.010}$	$-0.002^{+0.009}_{-0.009}$	$0.000^{+0.003}_{-0.003}$
	Λ_+	5.2	5.0	5.6	5.6	9.6	7.7	7.2	7.8	14.3
	Λ_-	5.3	5.1	5.2	5.2	9.3	8.3	7.4	7.3	13.8
$q\overline{q}$	ε_0	$-0.037^{+0.057}_{-0.063}$	$0.023^{+0.057}_{-0.056}$	$0.007^{+0.055}_{-0.054}$	$0.024^{+0.105}_{-0.039}$	$0.013^{+0.030}_{-0.028}$	$-0.019^{+0.028}_{-0.035}$	$-0.011^{+0.040}_{-0.037}$	$0.023^{+0.060}_{-0.036}$	$0.007^{+0.017}_{-0.010}$
	Λ_+	4.4	3.0	3.3	2.5	4.1	6.3	4.4	3.1	5.8
	Λ_-	2.8	3.9	3.6	4.9	5.7	3.8	3.8	5.5	10.3
combined	ε_0	$-0.003^{+0.017}_{-0.017}$	$-0.004^{+0.018}_{-0.018}$	$-0.002^{+0.017}_{-0.016}$	$0.002^{+0.016}_{-0.015}$	$0.000^{+0.006}_{-0.006}$	$0.000^{+0.007}_{-0.008}$	$0.000^{+0.009}_{-0.010}$	$0.000^{+0.009}_{-0.008}$	$0.000^{+0.003}_{-0.002}$
	Λ_+	5.8	5.7	5.7	5.5	9.5	8.4	7.4	7.7	14.0
	Λ_-	5.2	5.0	5.4	6.1	9.7	8.1	7.4	7.9	15.0
$b\overline{b}$	ε_0	$0.015^{+0.025}_{-0.027}$	$0.035^{+0.049}_{-0.068}$	$-0.154^{+0.277}_{-0.059}$	$-0.039^{+0.077}_{-0.048}$	$0.014^{+0.017}_{-0.024}$	$0.010^{+0.014}_{-0.018}$	$0.011^{+0.018}_{-0.019}$	$-0.046^{+0.187}_{-0.042}$	$-0.046^{+0.018}_{-0.010}$
	Λ_+	4.0	2.9	2.4	1.8	4.6	5.2	4.7	2.4	6.1
	Λ_-	4.8	1.7	2.0	2.8	2.1	6.0	5.7	2.9	4.0
$u\overline{u}$	ε_0	$0.021^{+0.039}_{-0.037}$	$0.033^{+0.069}_{-0.056}$	$0.069^{+0.152}_{-0.126}$	$0.001^{+0.126}_{-0.112}$	$0.010^{+0.020}_{-0.018}$	$0.015^{+0.034}_{-0.026}$	$0.012^{+0.023}_{-0.021}$	$0.033^{+0.105}_{-0.081}$	$0.005^{+0.011}_{-0.009}$
	Λ_+	3.1	1.5	1.9	2.2	4.4	3.1	4.1	2.3	3.1
	Λ_-	4.5	3.8	2.8	2.4	6.3	5.5	5.8	3.2	9.0
$d\overline{d}$	ε_0	$-0.023^{+0.041}_{-0.047}$	$-0.077^{+0.118}_{-0.184}$	$-0.040^{+0.124}_{-0.126}$	$0.077^{+0.149}_{-0.120}$	$-0.020^{+0.034}_{-0.155}$	$-0.015^{+0.026}_{-0.034}$	$-0.016^{+0.029}_{-0.035}$	$0.035^{+0.081}_{-0.089}$	$-0.015^{+0.026}_{-0.031}$
	Λ_+	4.3	3.1	2.6	1.8	4.9	5.5	5.0	2.5	6.4
	Λ_-	2.8	1.8	2.1	3.0	2.2	3.1	3.3	3.1	4.1
$u\overline{u}$+ $d\overline{d}$	ε_0	$0.020^{+0.087}_{-0.087}$	$0.054^{+0.098}_{-0.093}$	$0.020^{+0.087}_{-0.087}$	$0.054^{+0.098}_{-0.093}$	$0.029^{+0.064}_{-0.044}$	$0.001^{+0.042}_{-0.043}$	$0.037^{+0.069}_{-0.066}$	$0.037^{+0.069}_{-0.066}$	$0.009^{+0.030}_{-0.015}$
	Λ_+	2.5	2.2	2.5	2.2	3.0	3.9	2.7	2.7	4.5
	Λ_-	2.9	3.4	2.9	3.4	5.1	3.9	4.0	4.0	8.3

Table 10: Results of the contact interaction fits to the angular distributions for non-radiative $e^+e^- \to e^+e^-$, $e^+e^- \to \mu^+\mu^-$, $e^+e^- \to \tau^+\tau^-$, the cross-sections for $e^+e^- \to q\overline{q}$ and the measurements of R_b. Results at centre-of-mass energies of 161–172 GeV [1] are also included. The combined results include all leptonic angular distributions and the hadronic cross-sections. The numbers in square brackets are the values of $[\eta_{LL},\eta_{RR},\eta_{LR},\eta_{RL}]$ which define the models. ε_0 is the fitted value of $\varepsilon = 1/\Lambda^2$, $\Lambda_\pm$ are the 95% confidence level limits. The units of Λ are TeV, those of ε_0 are TeV^{-2}.

kinematic limit for direct production, such a new particle might be seen through a change of the total cross-section in the process $e^+e^- \to q\overline{q}$ via a t-channel exchange diagram. The classification of the various allowed leptoquark states is given in [32].

To search for new heavy particles coupling to quarks and leptons we perform a χ^2 fit between measured non-radiative hadronic cross-sections and model predictions, as described in detail in [1]. The hadronic cross-sections used are the values at 183 GeV and 130–136 GeV presented here, together with those at 161 and 172 GeV presented in [1]. Correlations between these measurements caused by common systematic errors are taken into account. We also perform fits to the $b\overline{b}$ cross-sections, considering all possible leptoquark couplings to the b quark. The predicted cross-section for $e^+e^- \to q\overline{q}$ including t-channel exchange of a leptoquark is calculated in [32]. Electroweak corrections are included as for the contact interaction fits, and Standard Model cross-sections are calculated using ZFITTER.

Figure 8 shows the 95% confidence limits obtained as a function of the mass m_X and the coupling constant g_L or g_R of the new particle, for scalar states. Results for the vector leptoquark states are shown in Fig. 9. We do not show limits on the S_0 (V_0) leptoquark with coupling g_R (g_L) because the effect of these particles on the hadronic cross-section at these energies is too small. For the states shown, the limits on the coupling, derived from hadronic cross-section measurements, typically lie in the range 0.15–0.6 for a mass of 200 GeV. Inclusion of data at 183 GeV has lowered these limits by about 20% compared with those obtained from lower energy data [1, 33]. The limits derived from $b\overline{b}$ cross-sections are generally somewhat more stringent than those obtained from the hadronic cross-sections.

As can be seen in the figures our analysis is sensitive to leptoquark masses much higher than the beam energy. Direct searches at the Tevatron can exclude scalar and vector leptoquarks with Yukawa couplings down to $\mathcal{O}(10^{-7})$ up to masses of ≈ 225 GeV [34]. Our limits extend this excluded region for large couplings.

4.2.2 Particles Coupling to Leptons

The cross-section for the production of two leptons can also be affected by the presence of new heavy particles which couple to leptons. Three cases can be distiguished: the new particles might contribute to the measured cross-section via the s-channel, via a t-channel exchange, or both channels may be present. In order to test the sensitivity of the OPAL data to such interactions, we have chosen to use sneutrinos with R-parity violating couplings as an example. Their coupling to leptons is given by the term $\lambda_{ijk} L^i_L L^j_L \overline{E}^k_R$ of the superpotential [35], where the indices i, j, k denote the family of the particles involved, L^i_L and L^j_L are the SU(2) doublet lepton superfields and $\overline{E}^k_R$ denotes an antilepton singlet superfield. The couplings λ_{ijk} are non-vanishing only for $i < j$, so at least two different generations of leptons are coupled in purely leptonic vertices. We consider three typical cases in our analysis in order to illustrate the sensitivity of each of the leptonic channels:

- the presence of a $\tilde{\nu}_e$ with coupling λ_{131}, giving rise to a change in the $\tau^+\tau^-$ cross-section due to t-channel exchange;
- the presence of a $\tilde{\nu}_\tau$ which interacts via the coupling λ_{131} giving rise to a change in the e^+e^- cross-section via an s-channel and a t-channel process; the limits obtained for this case could equally apply to a $\tilde{\nu}_\mu$ interacting via the coupling λ_{121};

- a $\tilde{\nu}_\tau$ with the couplings λ_{131} and λ_{232} both different from zero. In the analysis both couplings are assumed to be of equal size[3]. Such a scenario gives rise to a modified $\mu^+\mu^-$ cross-section due to an s-channel exchange of the sneutrino.

To calculate the differential cross-sections for these processes we use the formulae in [36], taking radiative corrections into account as in the contact interaction analysis.

In the case of the $\tau^+\tau^-$ cross-section only the t-channel exchange of a $\tilde{\nu}_e$ is involved. We perform a maximum likelihood fit which compares the model prediction with the observed number of events having $s'/s > 0.7225$. Systematic errors are taken into account by multiplying the likelihood by a factor $(1 + r)$ where r is distributed according to a Gaussian with a width given by the systematic error on the data sample. This is the method used to extract limits on four-fermion contact interactions in this paper and in [1,28]. For each mass, the 95% confidence level limit on the coupling is obtained as the value of λ corresponding to a change in negative log likelihood of 1.92 with respect to the minimum.

The cases where an s-channel diagram is involved are especially interesting. A narrow peak in the cross-section when the centre-of-mass energy equals the mass of the sneutrino is then predicted, since the sneutrinos are expected to have a small width ($\lesssim$ 1 GeV [36]). In order to improve the sensitivity for sneutrino masses which lie between the centre-of-mass energies of LEP, a fit method has been developed which scans the complete s'-distribution of the recorded data. The $\sqrt{s'}$ distributions at 183 GeV are shown in Fig. 1; a sneutrino of mass m would be expected to produce a peak in the $\sqrt{s'}$ distribution at $\sqrt{s'} \simeq m$ for a process receiving a contribution from s-channel sneutrino production. We calculate limits on the coupling as a function of sneutrino mass as follows. For each mass m, we consider a window of width ± 2.5 GeV around $\sqrt{s'} = m$, and calculate the number of signal and Standard Model background events expected in this interval. We assume the efficiency for detecting signal events (within the $|\cos\theta|$ acceptance of each channel) is the same as that for Standard Model events at the same s'. The size of the window is chosen to be such that at least 60% of events of mass m are reconstructed within the window. In this interval a maximum likelihood fit is performed which compares the model prediction with the measured data. Systematic errors are considered in the same way as for the t-channel case.

In the case of the e^+e^- cross-section the presence of both an s-channel and a t-channel diagram is assumed, and we consider two contributions to the likelihood function: one arising from the $\sqrt{s'}$ interval around m and one from the $s'/s > 0.7225$ region. In cases where these intervals overlap only the contribution from the interval around m was considered, as the s-channel diagram is expected to dominate. For this analysis, we use electron pairs with $|\cos\theta_{e^-}| < 0.7$, with no cut on acollinearity. The Standard Model prediction in each s' window is calculated using Monte Carlo events generated with BHWIDE [37]. Systematic errors on the Standard Model prediction are assessed by reweighting the Monte Carlo events to the acollinearity distribution predicted by ALIBABA.

At large values of λ the limits can be improved by including measurements of forward-backward asymmetry in the fit. This is achieved by adding a term to the negative log likelihood of the form

$$-\ln P = \sum_i \ln \Delta A_i + \frac{(A_i^{\rm th} - A_i^{\rm meas})^2}{2(\Delta A_i)^2}$$

[3]Both couplings violate the same lepton flavours so that this scenario is compatible with the experimental observation of lepton number conservation.

where the sum runs over the measurements at different energies. $A_i^{\rm th}$ is the theoretical prediction of the asymmetry, including the effects of new physics, $A_i^{\rm meas}$ is the measured value and ΔA_i the error on the measurement. We have calculated limits both including and excluding measurements of asymmetry for non-radiative events. While the former are valid for the exchange of a scalar particle with a width less than or equal to 1 GeV, the latter are less model dependent and could be reinterpreted in terms of the exchange of a vector particle with appropriate modifications to the coupling constant. For the $\rm e^+e^-$ and $\mu^+\mu^-$ channels, the inclusion of asymmetry values has a very small effect on the limits, therefore we present only limits excluding asymmetry measurements in order not to lose generality. In the case of the $\tau^+\tau^-$ channel the limits on λ are larger and we present results both including and excluding the asymmetry measurements.

In all cases, we include in the fits the data at 183 and 130–136 GeV presented here and the data at 161 and 172 GeV presented in [1]. In the analysis of the $\tau^+\tau^-$ channel we use the measured non-radiative cross-sections and asymmetries, whereas for the $\mu^+\mu^-$ and $\rm e^+e^-$ channels we use the full $\sqrt{s'}$ distributions as described above. We present limits on the coupling as a function of sneutrino mass for each of the three cases.

The limits on λ_{131} derived from the $\tau^+\tau^-$ data are shown in Fig. 10. As only a t-channel contribution is involved, the limit on λ varies smoothly with the $\tilde{\nu}$ mass, from about 0.5 at 100 GeV to 1.2 at 400 GeV. The inclusion of asymmetry data improves the limit by about 0.1. The limits on λ_{131} derived from the $\rm e^+e^-$ data are shown in Fig. 11. They are in the range 0.02 – 0.1 for $100 < m < 200$ GeV, rising to 0.27 at 300 GeV. Figure 12 shows limits on $\lambda_{131} = \lambda_{232}$ derived from the $\mu^+\mu^-$ data. These are in the range 0.02 – 0.1 for $100 < m < 200$ GeV, rising to 0.3 at 300 GeV. By introducing the s' distributions in our fits we find the sensitivity in the $\rm e^+e^-$ and $\mu^+\mu^-$ channels has been improved for masses between the LEP centre-of-mass energy points. The fine structure in the region $m < 200$ GeV results from fluctuations in the s' distributions.

Direct searches [38] for sneutrinos with R-parity violating couplings can conservatively exclude a $\tilde{\nu}_\tau$ with mass less than 49 GeV and a $\tilde{\nu}_e$ with mass less than 72 GeV. Our results place limits on the couplings for higher masses.

5 Conclusions

We have presented new measurements of cross-sections and asymmetries for hadron and lepton pair production in $\rm e^+e^-$ collisions at centre-of-mass energies of 183 and 130–136 GeV, and combined the 130–136 GeV results with our measurements from earlier data [1]. The results, for both inclusive fermion-pair production and for non-radiative events, are in good agreement with Standard Model expectations. From these and earlier measurements we derive a value for the electromagnetic coupling constant $1/\alpha_{\rm em}(169.34\ {\rm GeV}) = 127.8^{+4.1}_{-3.6}$.

The measurements have been used to improve existing limits on new physics. In the context of a four-fermion contact interaction we have improved the limits on the energy scale Λ from typically 2–7 TeV to 2–10 TeV, assuming $g^2/4\pi = 1$. In explicit searches for new particles coupling to quarks and leptons we obtain limits on the coupling in the range 0.15–0.6 for a mass of about 200 GeV, some 20% lower than those obtained from data at centre-of-mass energies up to 172 GeV. We have also presented limits on new particles such as sneutrinos in supersymmetric theories with R-parity violation which couple to leptons only. Sensitivity to

sneutrino masses between the centre-of-mass energy points of LEP has been improved by using a complete scan of the s' distribution for processes involving an s-channel diagram. In these cases, limits on the couplings in the range $0.02 - 0.1$ are obtained for $100 < m < 200$ GeV.

Acknowledgements

We thank R. Rückl for helpful discussions on setting limits on R-parity violating sneutrino couplings.

We particularly wish to thank the SL Division for the efficient operation of the LEP accelerator at all energies and for their continuing close cooperation with our experimental group. We thank our colleagues from CEA, DAPNIA/SPP, CE-Saclay for their efforts over the years on the time-of-flight and trigger systems which we continue to use. In addition to the support staff at our own institutions we are pleased to acknowledge the
Department of Energy, USA,
National Science Foundation, USA,
Particle Physics and Astronomy Research Council, UK,
Natural Sciences and Engineering Research Council, Canada,
Israel Science Foundation, administered by the Israel Academy of Science and Humanities,
Minerva Gesellschaft,
Benoziyo Center for High Energy Physics,
Japanese Ministry of Education, Science and Culture (the Monbusho) and a grant under the Monbusho International Science Research Program,
German Israeli Bi-national Science Foundation (GIF),
Bundesministerium für Bildung, Wissenschaft, Forschung und Technologie, Germany,
National Research Council of Canada,
Research Corporation, USA,
Hungarian Foundation for Scientific Research, OTKA T-016660, T023793 and OTKA F-023259.

References

[1] OPAL Collab., K. Ackerstaff et al., Eur. Phys. J. **C2** (1998) 441.

[2] ALEPH Collab., D. Buskulic et al., Phys. Lett. **B378** (1996) 373;
L3 Collab., M. Acciarri et al., Phys. Lett. **B370** (1996) 195;
L3 Collab., M. Acciarri et al., Phys. Lett. **B407** (1997) 361.

[3] L3 Collab., M. Acciarri et al., Phys. Lett. **B414** (1997) 373.

[4] OPAL Collab., K. Ahmet et al., Nucl. Instr. Meth. **A305** (1991) 275.

[5] S. Anderson et al., Nucl. Instr. Meth. **A403** (1998) 326.

[6] B.E. Anderson et al., IEEE Trans. Nucl. Sci. **41** (1994) 845.

[7] M. Arignon et al., Nucl. Instr. Meth. **313** (1992) 103;
M. Arignon et al., Nucl. Instr. Meth. **333** (1993) 330.

[8] J.T. Baines et al., Nucl. Instr. Meth. **A325** (1993) 271;
D.G. Charlton, F. Meijers, T.J. Smith, P.S. Wells, Nucl. Instr. Meth. **A325** (1993) 129.

[9] The LEP Energy Working Group, *Preliminary LEP energy calibration for 1997 data*, LEP Energy Working Group 98/01, March 1998.

[10] J. Fujimoto et al., Comput. Phys. Commun. **100** (1997) 128.

[11] T. Sjöstrand, Comput. Phys. Commun. **82** (1994) 74.

[12] J. Allison et al., Nucl. Instr. Meth. **A317** (1992) 47.

[13] OPAL Collab., Eur. Phys. J. **C1** (1998) 395.

[14] D. Bardin et al., CERN-TH 6443/92 (May 1992); Phys. Lett. **B255** (1991) 290; Nucl. Phys. **B351** (1991) 1; Z. Phys. **C44** (1989) 493;
we use ZFITTER version 5.0 with default parameters, except `BOXD`=1, `CONV`=1, `INTF`=0 and `FINR`=0, and with the following input parameters: $m_{\rm Z}$=91.1863 GeV, $m_{\rm top}$=175 GeV, $m_{\rm Higgs}$=300 GeV, $\alpha_{\rm em}(m_{\rm Z})$=1/128.896, $\alpha_{\rm s}(m_{\rm Z})$=0.118.

[15] W. Beenakker et al., Nucl. Phys. **B349** (1991) 323.

[16] OPAL Collab., P.D. Acton et al., Z. Phys. **C58** (1993) 219.

[17] OPAL Collab., R. Akers et al., Z. Phys. **C61** (1994) 19.

[18] OPAL Collab., G. Alexander et al., Z. Phys. **C52** (1991) 175.

[19] The LEP Experiments: ALEPH, DELPHI, L3 and OPAL, Nucl. Instr. Meth. **A378** (1996) 101.

[20] D. Bardin et al., Nucl. Phys. Proc. Suppl. **37B** (1994) 148.

[21] J. Hilgart, R. Kleiss, F. Le Diberder, Comp. Phys. Comm. **75** (1993) 191.

[22] HRS Collab., D. Bender et al., Phys. Rev. **D31** (1985) 1;
MAC Collab., E. Fernandez et al., Phys. Rev. **D31** (1985) 1537;
PLUTO Collab., C. Berger et al., Phys. Lett. **B81** (1979) 410;
CELLO Collab., H.J. Behrend et al., Phys. Lett.**B183** (1987) 400;
JADE Collab., W. Bartel et al., Phys. Lett. **B129** (1983) 145;
JADE Collab., W. Bartel et al., Phys. Lett.**B160** (1985) 337;
MARKJ Collab., B. Adeva et al., Phys. Rev. Lett. **50** (1983) 799;
MARKJ Collab., B. Adeva et al., Phys. Rev. **D34** (1986) 681;
TASSO Collab., R. Brandelik et al., Phys. Lett. **B113** (1982) 499;
TASSO Collab., M. Althoff et al., Phys. Lett. **B138** (1984) 441;
AMY Collab., T. Mori et al., Phys. Lett. **B218** (1989) 499;
TOPAZ Collab., I. Adachi et al., Phys. Rev. Lett. **60** (1988) 97;
VENUS Collab., H. Yoshida et al., Phys. Lett. **B198** (1987) 570;
TOPAZ Collab., K. Miyabayashi et al., Phys. Lett. **B347** (1995) 171.

[23] TOPAZ Collab., I. Levine et al., Phys. Rev. Lett. **78** (1997) 424.

[24] M. Kobel, *Direct Measurements of the Electromagnetic Coupling Constant at Large* q^2, FREIBURG-EHEP 97-13, Contributed paper to the XVIII International Symposium on Lepton Photon Interactions, Hamburg, July 1997.

[25] M.E. Cage et al., IEEE Trans. Instrum. Meth. **38** (1989) 284.

[26] E. Eichten, K. Lane, M. Peskin, Phys. Rev. Lett. **50** (1983) 811.

[27] See for example *Contact interactions and new heavy bosons at HERA: a model independent analysis*, P. Haberl, F. Schrempp, H.U. Martyn, in Proceedings, Physics at HERA, **vol. 2**, (1991) 1133.

[28] OPAL Collab., G. Alexander et al., Phys. Lett. **B387** (1996) 432.

[29] G.J. Gounaris, D.T. Papadamou, F.M. Renard, Phys. Rev. **D56** (1997) 3970.

[30] W. Buchmüller, R. Rückl, D. Wyler, Phys. Lett. **B191** (1987) 442;
J. L. Hewett, T. Rizzo, Phys. Rev. **D36** (1987) 3367.

[31] For an overview see for example H. Dreiner, G.G. Ross, Nucl. Phys. **B410** (1993) 188;
G.G. Ross, J.W.F. Valle, Phys. Lett. **B151** (1985) 375.

[32] J. Kalinowski, R. Rückl, H. Spiesberger, P.M. Zerwas, Z. Phys. **C74** (1997) 595.

[33] L3 Collab., M. Acciarri et al., *Search for New Physics Phenomena in Fermion-Pair Production at LEP*, CERN-EP/98-031, February 1998, to be published in Phys. Lett. B.

[34] CDF Collab., F. Abe et al., Phys. Rev. **D48** (1993) 3939;
CDF Collab., F. Abe et al., Phys. Rev. Lett. **75** (1995) 1012;
CDF Collab., F. Abe et al., Phys. Rev. Lett. **78** (1997) 2906;
D0 Collab., S. Abachi et al., Phys. Rev. Lett. **75** (1995) 3618;
D0 Collab., B. Abbott et al., Phys. Rev. Lett. **79** (1997) 4321.

[35] J. Wess, J. Bagger, *Supersymmetry and Supergravity* (Princeton University Press, 1983);
H.P. Nilles, Phys. Rep. **110** (1984) 1;
H.E. Haber, G.E. Kane, Phys. Rep. **117** (1985) 75;
R. Barbieri, Riv. Nuovo Cim. **11** (1988) 1;
P. West, *Introduction to Supersymmetry and Supergravity* (World Scientific, 1986).

[36] J. Kalinowski, R. Rückl, H. Spiesberger, P.M. Zerwas, Phys. Lett. **B406** (1997) 314.

[37] S. Jadach, W. Placzek, B.F.L. Ward, Phys. Lett. **B390** (1997) 298.

[38] ALEPH Collab., R. Barate et al., *Search for Supersymmetry with a dominant R-Parity violating* $LL\overline{E}$ *Coupling in* e^+e^- *Collisions at centre-of-mass energies of 130 GeV to 172 GeV*, CERN-PPE/97-151, December 1997, submitted to Eur. Phys. J. C.

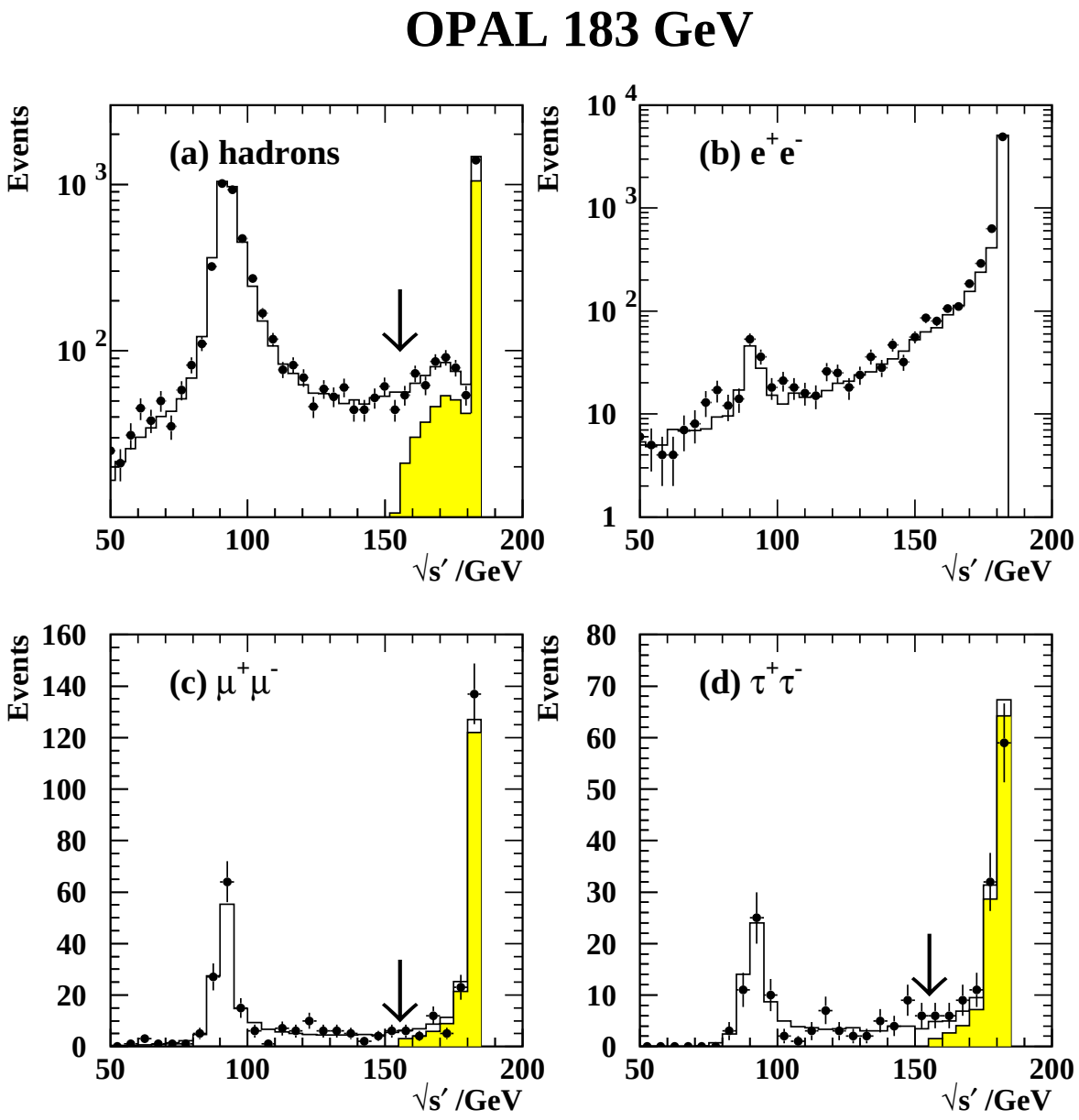

Figure 1: The distributions of reconstructed $\sqrt{s'}$ for (a) hadronic events, (b) electron pair events with $|\cos\theta_{e^+}| < 0.9$, $|\cos\theta_{e^-}| < 0.9$ and $\theta_{\rm acol} < 170°$, (c) muon pair and (d) tau pair events at 182.69 GeV. In each case, the points show the data and the histogram the Monte Carlo prediction, normalized to the integrated luminosity of the data, with the contribution from events with true $s'/s > 0.7225$ shaded in (a), (c) and (d). The arrows in (a), (c) and (d) show the position of the cut used to select 'non-radiative' events.

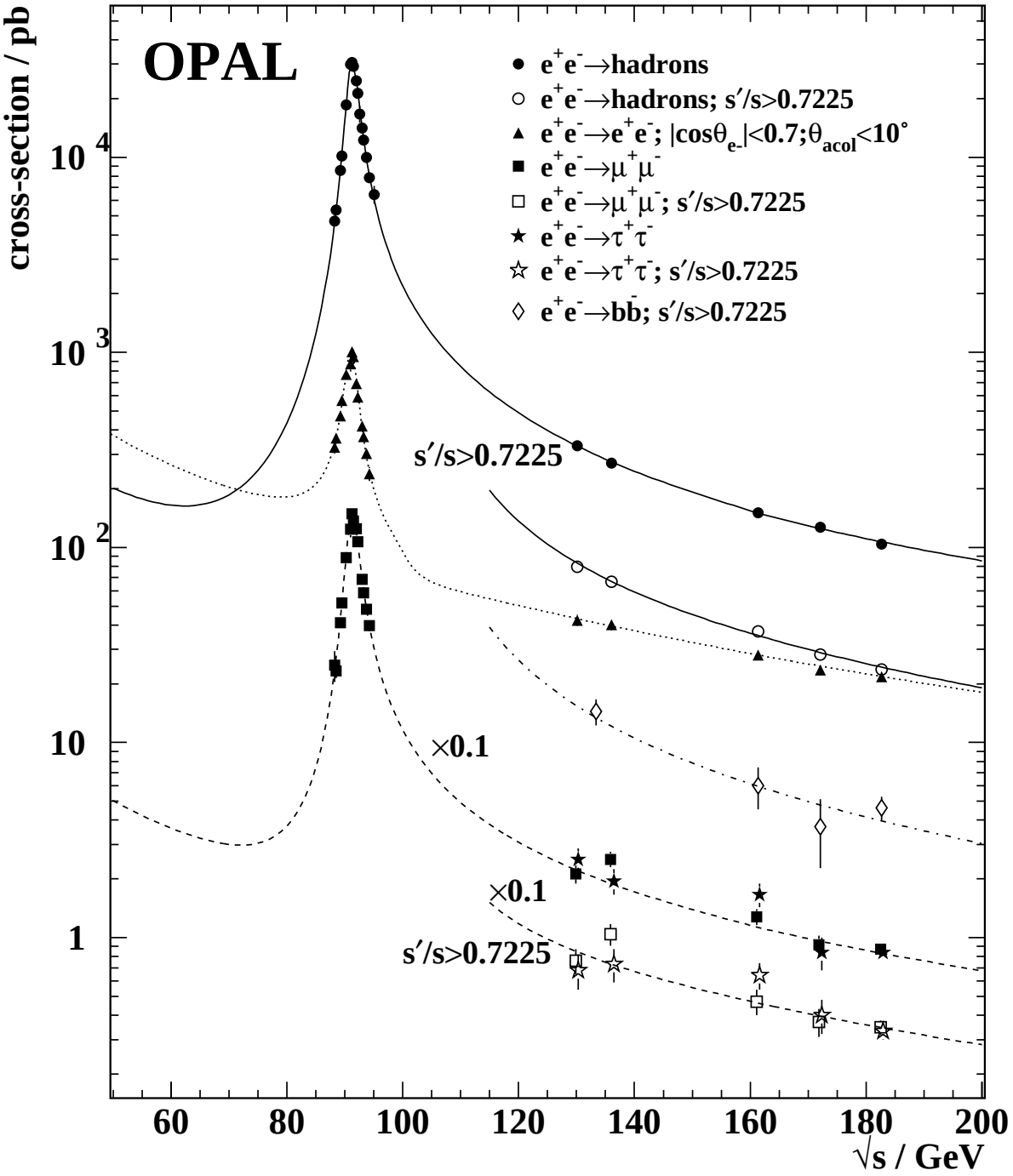

Figure 2: Measured total cross-sections ($s'/s > 0.01$) for different final states at lower energies [1, 16–18], and this analysis. Cross-section measurements for hadrons, $b\overline{b}$, $\mu^+\mu^-$ and $\tau^+\tau^-$ for $s'/s > 0.7225$ from this analysis and from [1] are also shown; the latter have been corrected from $s'/s > 0.8$ to $s'/s > 0.7225$ by adding the prediction of ZFITTER for this difference before plotting. The cross-sections for $\mu^+\mu^-$ and $\tau^+\tau^-$ production have been reduced by a factor of ten for clarity. The curves show the predictions of ZFITTER for hadronic (solid), $b\overline{b}$ (dot-dashed), $\mu^+\mu^-$ and $\tau^+\tau^-$ (dashed) final states and that of ALIBABA for the e^+e^- final state (dotted).

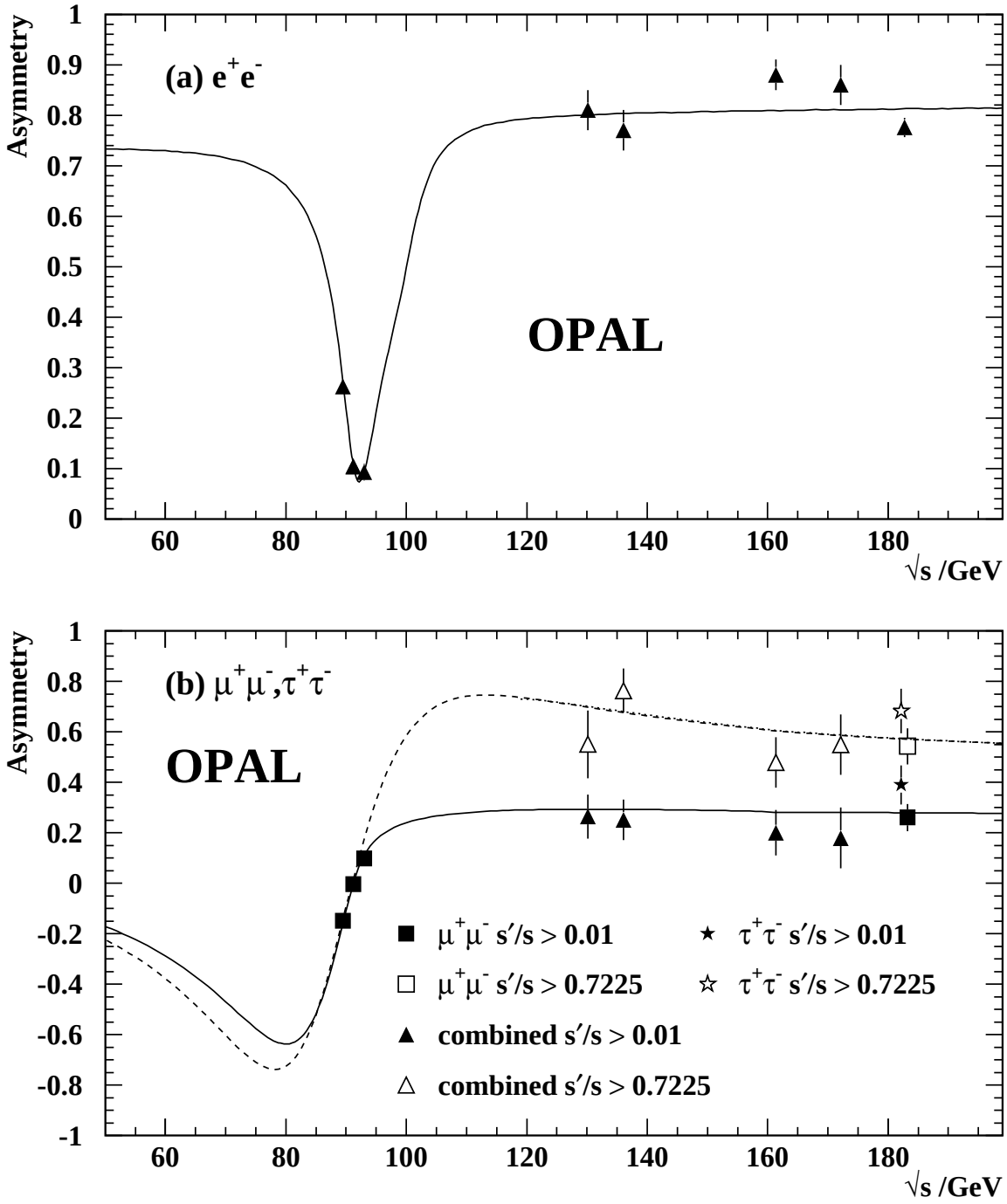

Figure 3: (a) Measured forward-backward asymmetry for electron pairs with $|\cos\theta_{e^-}| < 0.7$ and $\theta_{\rm acol} < 10^\circ$, as a function of $\sqrt{s}$. The curve shows the prediction of ALIBABA. (b) Measured asymmetries for all ($s'/s > 0.01$) and non-radiative ($s'/s > 0.7225$) samples as functions of $\sqrt{s}$ for $\mu^+\mu^-$ and $\tau^+\tau^-$ events. The curves show ZFITTER predictions for $s'/s > 0.01$ (solid) and $s'/s > 0.7225$ (dotted), as well as the Born-level expectation without QED radiative effects (dashed). The expectation for $s'/s > 0.7225$ lies very close to the Born curve, such that it appears indistinguishable on this plot.

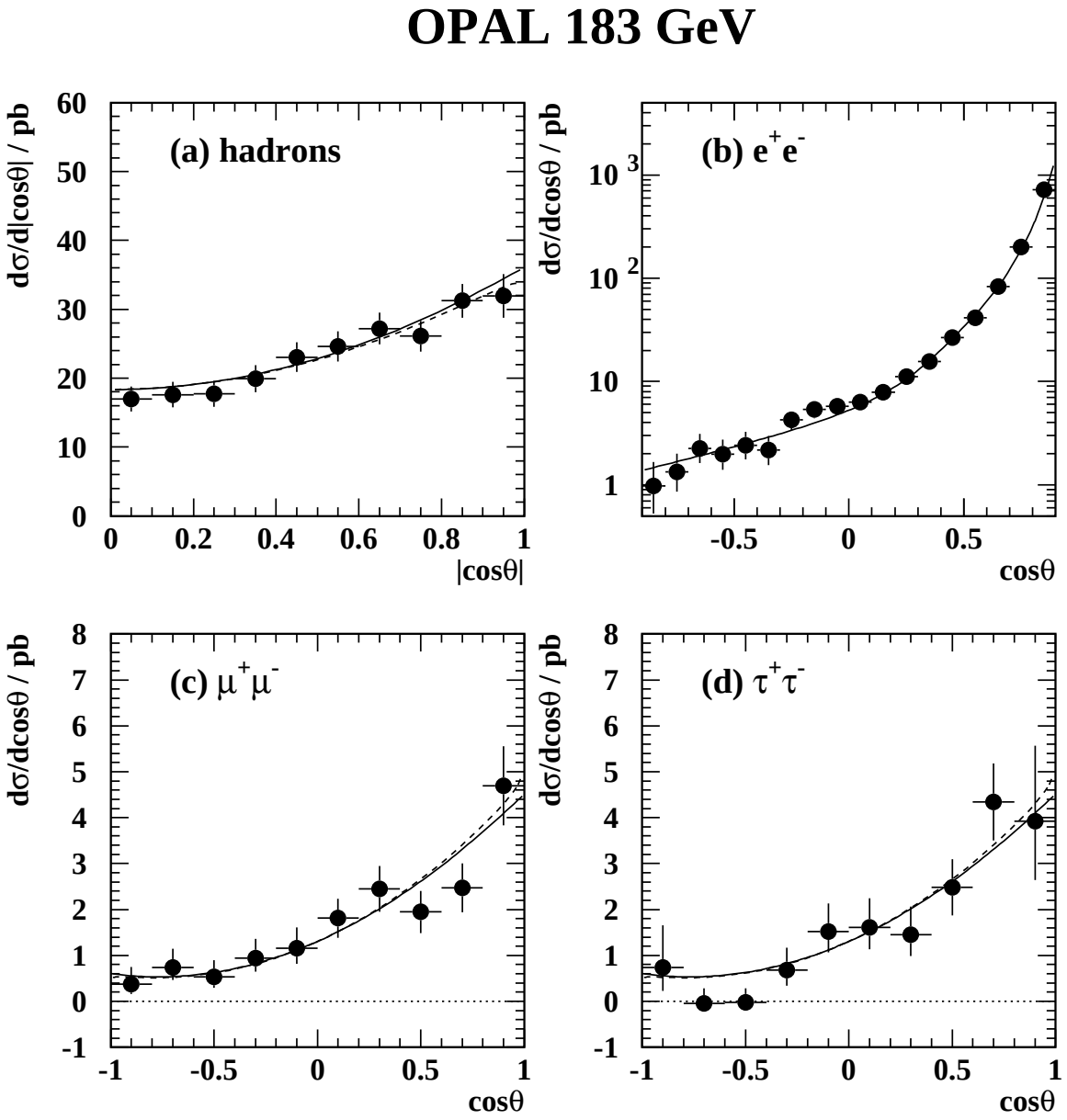

Figure 4: Angular distributions for (a) hadronic events with $s'/s > 0.7225$, (b) e^+e^- events with $\theta_{\rm acol} < 10°$, (c) $\mu^+\mu^-$ events with $s'/s > 0.7225$ and (d) $\tau^+\tau^-$ events with $s'/s > 0.7225$. The points show the 183 GeV data, corrected to no interference between initial- and final-state radiation in (a), (c) and (d). The curve in (b) shows the prediction of ALIBABA, while the curves in (a), (c) and (d) show the predictions of ZFITTER with no interference between initial- and final-state radiation (solid) and with interference (dashed).

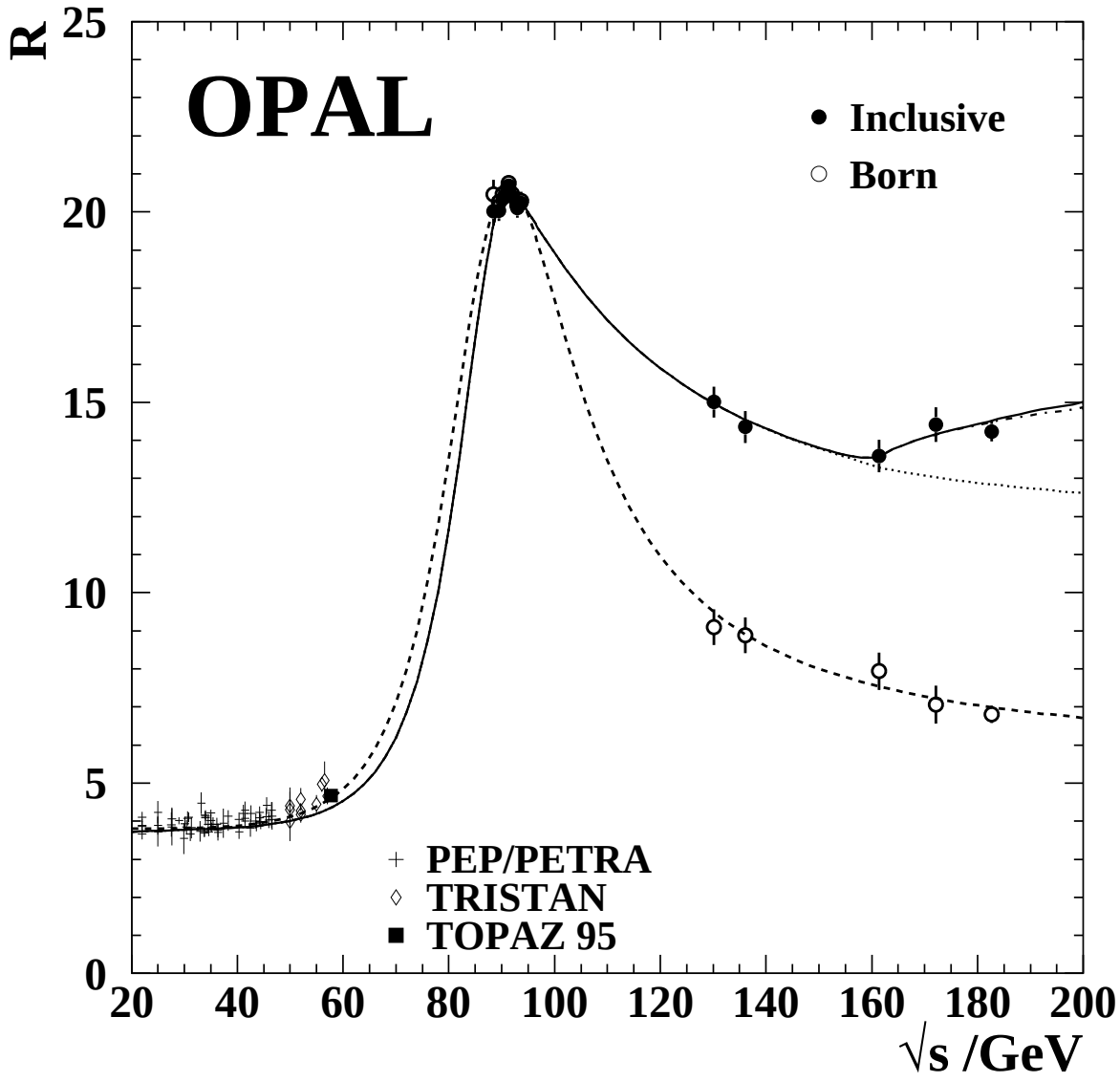

Figure 5: Ratio of measured hadronic cross-sections to theoretical muon pair cross-sections as a function of centre-of-mass energy. Values are shown for the inclusive cross-section, $\sigma(\mathrm{q\overline{q}X})$ and for the Born level cross-section. The dotted and dashed curves show the predictions of ZFITTER for these cross-sections, while the solid curve also includes the contributions from W-pairs calculated using GENTLE [20] and from Z-pairs calculated using FERMISV [21]. The dot-dashed curve is the total excluding the Z-pair contribution. Measurements at lower energies are from references [1, 16–18, 22].

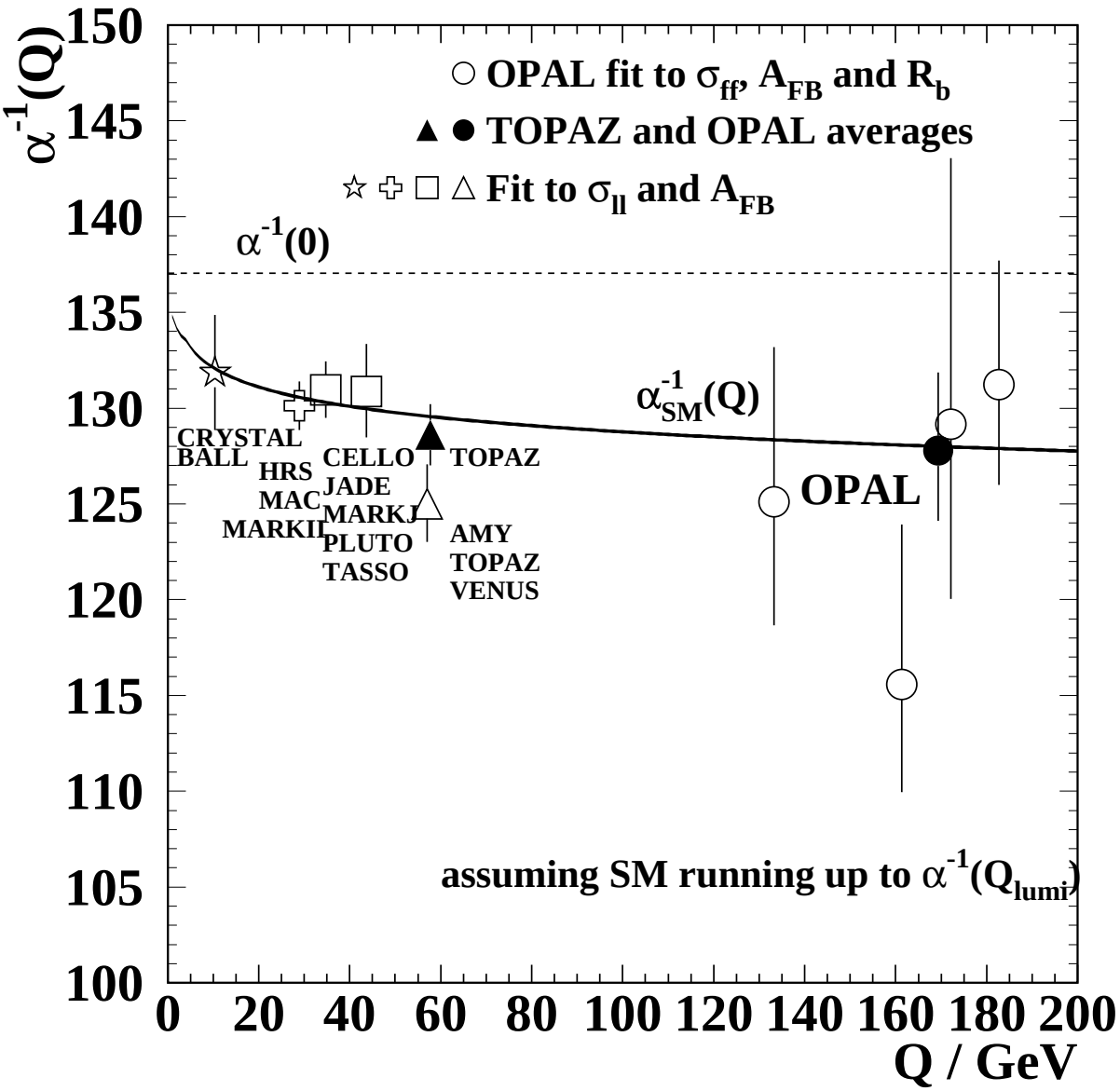

Figure 6: Fitted values of $1/\alpha_{\rm em}$ as a function of Q, which is $\sqrt{s}$ for the OPAL fits. The open circles show the results of fits to OPAL data at each centre-of-mass energy, the closed circle the result of the combined fit in which $\alpha_{\rm em}$ runs with a slope corresponding to its fitted value. The OPAL results at 161 and 172 GeV are from [1]. Values obtained by the TOPAZ experiment [23] and from fits to measurements of leptonic cross-sections and asymmetries at the DORIS, PEP, PETRA and TRISTAN e^+e^- storage rings [24] are also shown. All measurements rely on assuming the Standard Model running of $\alpha_{\rm em}$ for $Q_{\rm lumi}$ below 5 GeV. The solid line shows the Standard Model expectation, with the thickness representing the uncertainty, while the value of $1/\alpha_{\rm em}(0)$ is shown by the dashed line.

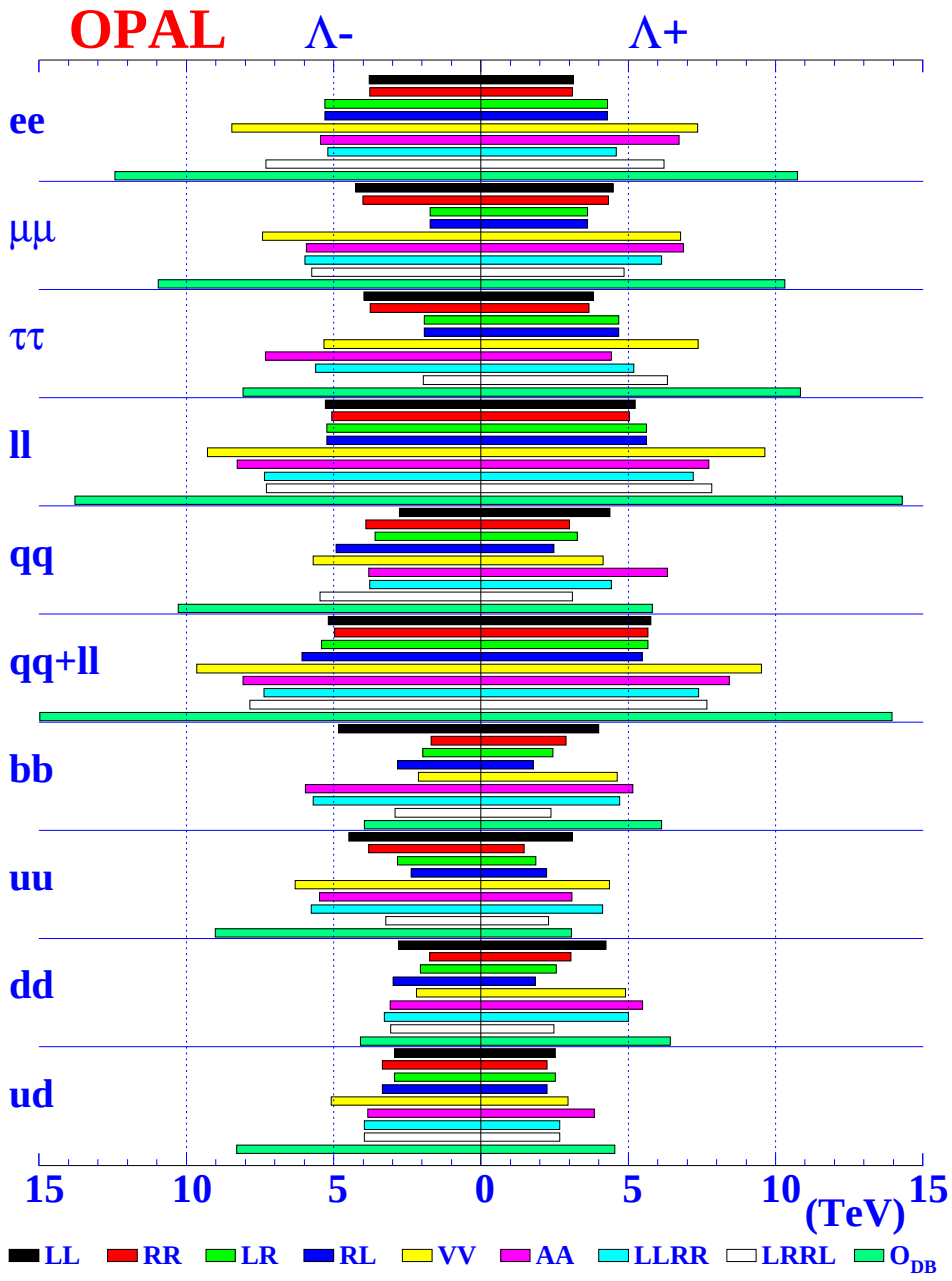

Figure 7: 95% confidence level limits on the energy scale Λ resulting from the contact interaction fits. For each channel, the bars from top to bottom indicate the results for models LL to $\overline{\mathcal{O}}_{\rm DB}$ in the order given in the key.

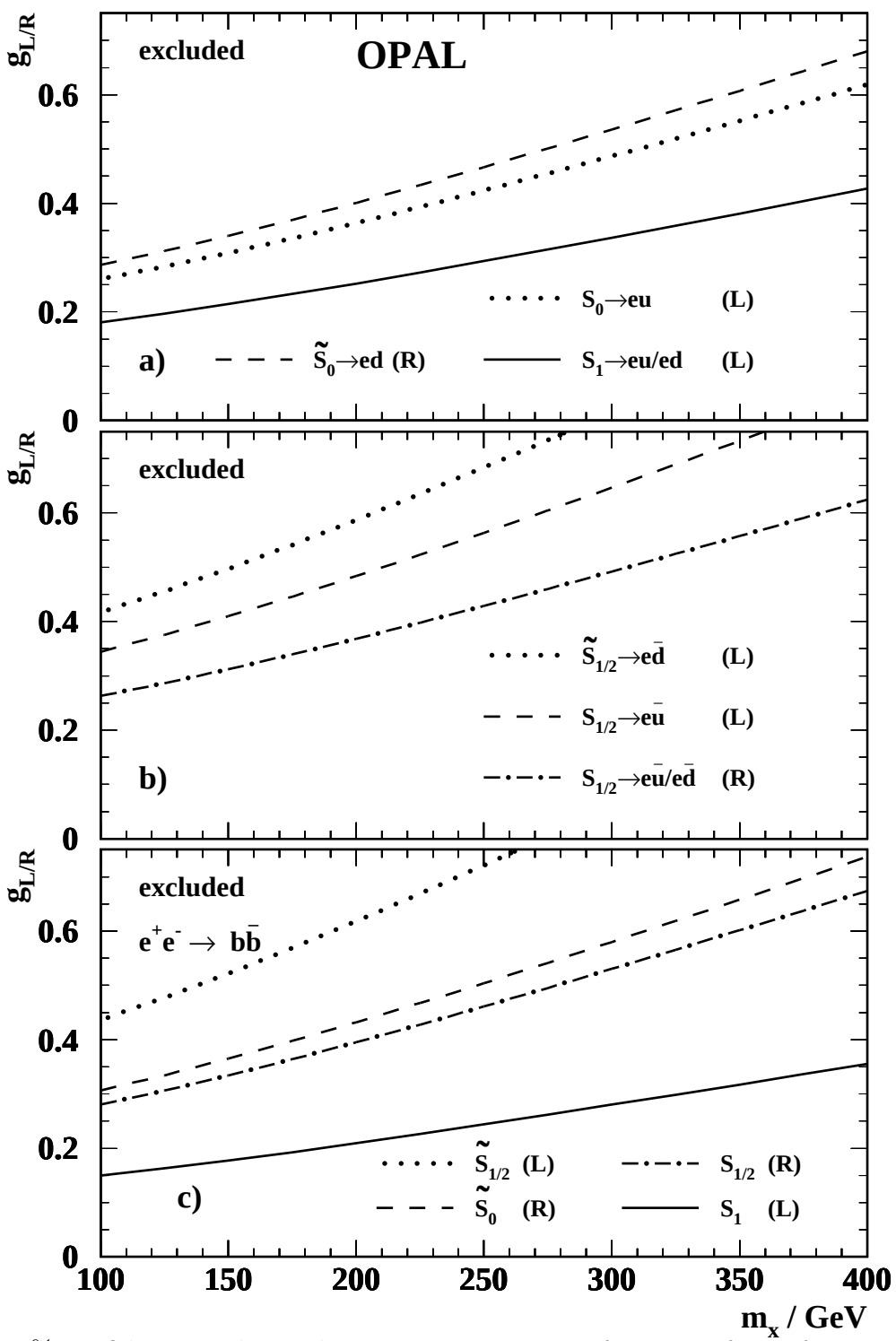

Figure 8: 95% confidence exclusion limits on g_L or g_R as a function of m_X, for various possible scalar leptoquarks. (a) and (b) show limits on leptoquarks coupling to a single quark family, derived from the hadronic cross-sections. (c) shows limits on leptoquarks coupling to b quarks only, derived from the $b\overline{b}$ cross-sections. The excluded regions are above the curves in all cases. The letter in parentheses after the different leptoquark types indicates the chirality of the lepton involved in the interaction. The limits on the S_0 and $\tilde{S}_{1/2}$ leptoquarks can be interpreted as limits on R-parity violating $\tilde{d}_R$ and $\tilde{u}_L$ squarks respectively.

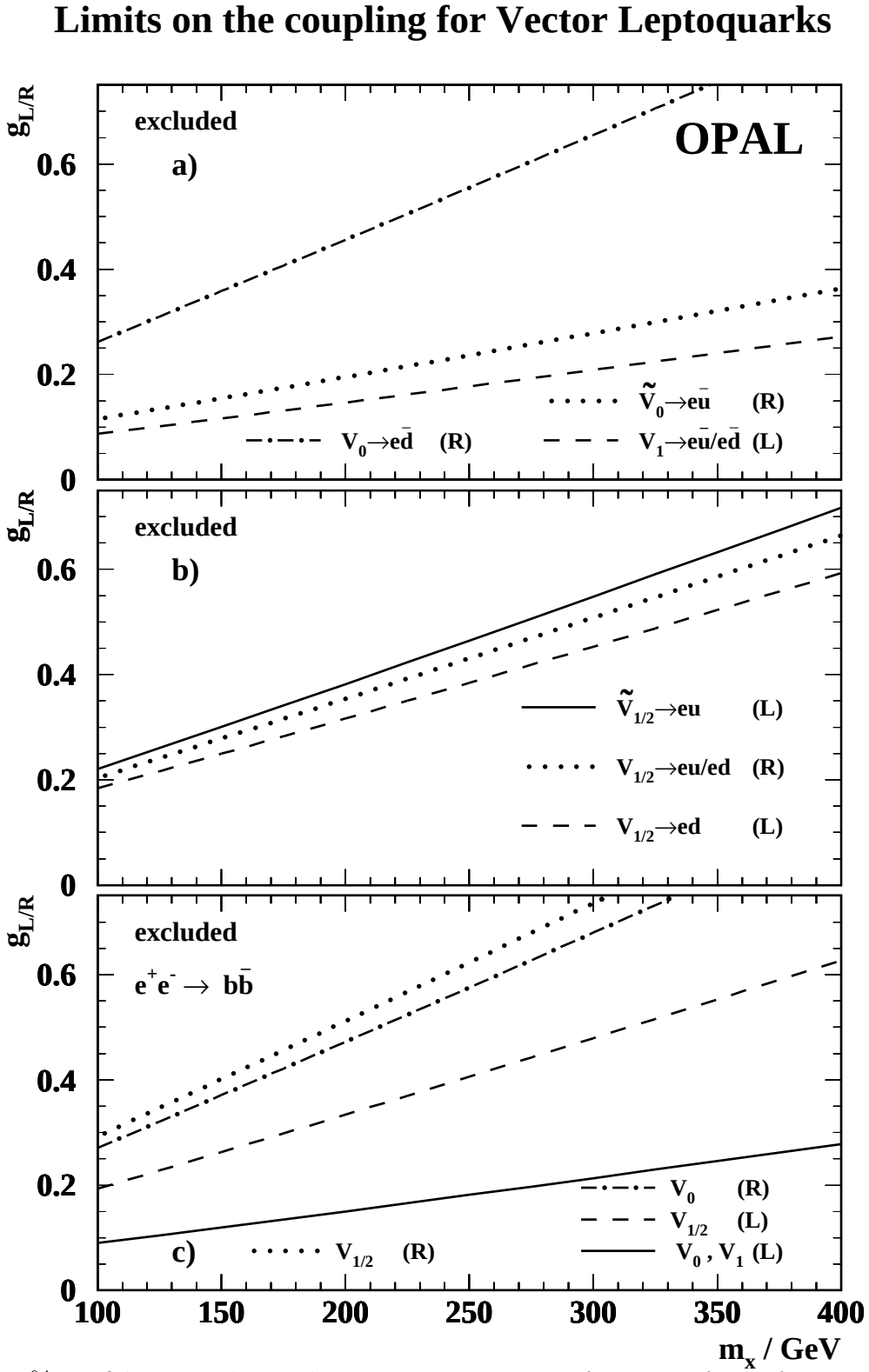

Figure 9: 95% confidence exclusion limits on g_L or g_R as a function of m_X, for various possible vector leptoquarks. (a) and (b) show limits on leptoquarks coupling to a single quark family, derived from the hadronic cross-sections. (c) shows limits on leptoquarks coupling to b quarks only, derived from the $b\overline{b}$ cross-sections. The excluded regions are above the curves in all cases. The letter in parentheses after the different leptoquark types indicates the chirality of the lepton involved in the interaction.

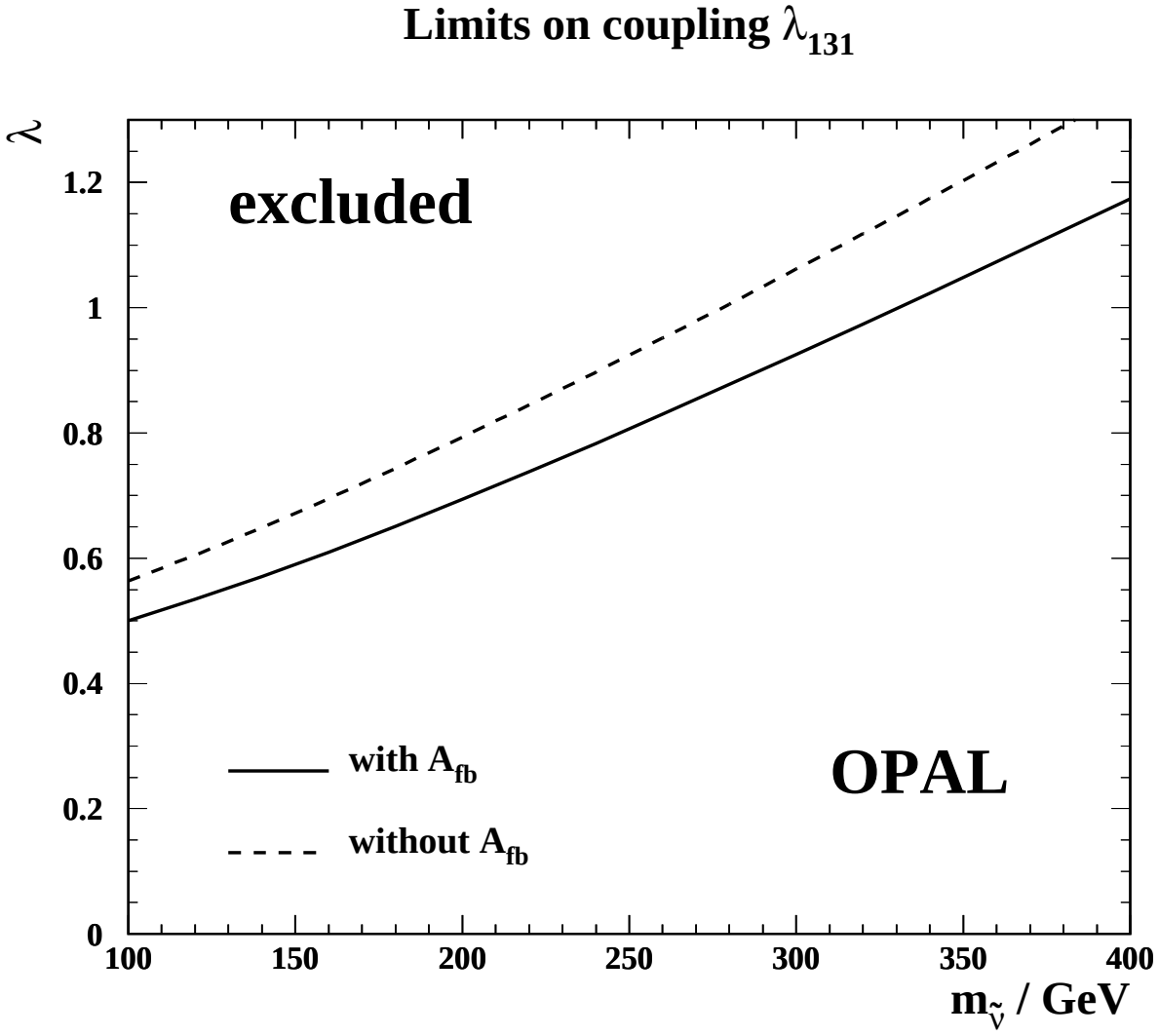

Figure 10: 95% confidence exclusion limit on λ_{131} as a function of sneutrino mass $m_{\tilde{\nu}}$, derived from $\tau^+\tau^-$ cross-section and asymmetry data. The region above the solid line is excluded. The dashed line shows the limit determined from cross-section data alone.

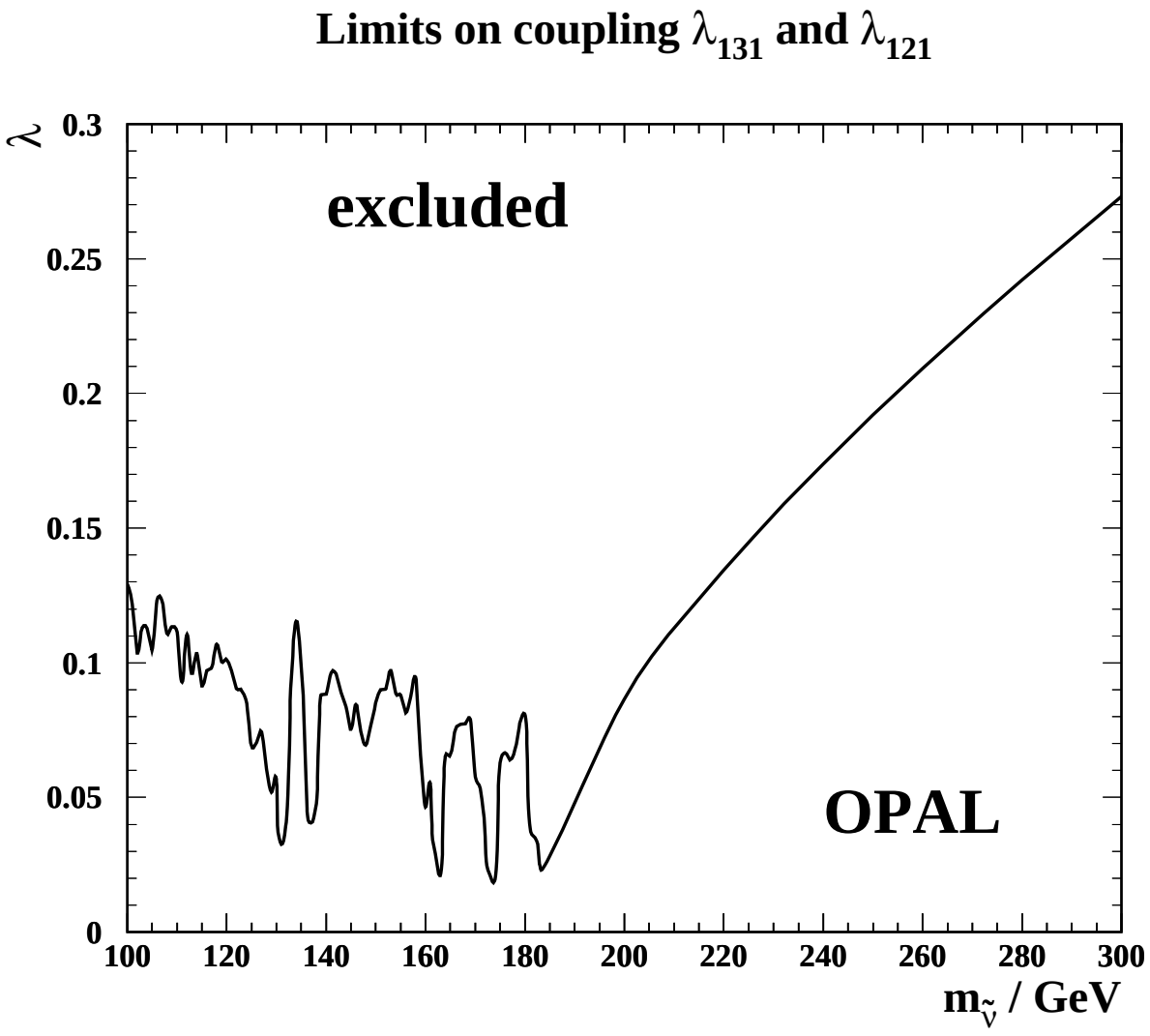

Figure 11: 95% confidence exclusion limits on λ_{131} (or λ_{121}) as a function of sneutrino mass $m_{\tilde{\nu}}$, derived from e^+e^- s' distributions. The region above the solid line is excluded.

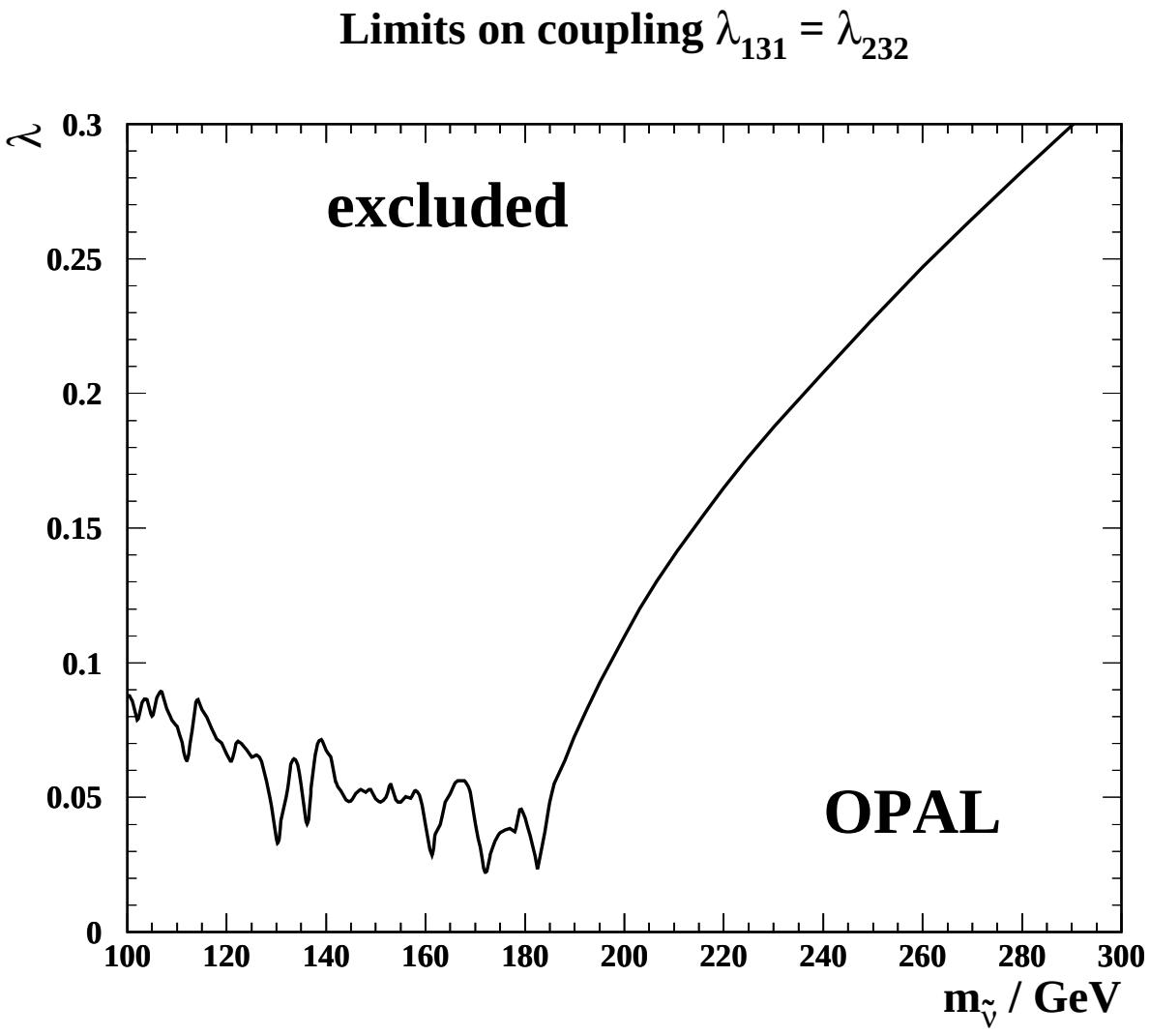

Figure 12: 95% confidence exclusion limit on $\lambda_{131} = \lambda_{232}$ as a function of sneutrino mass $m_{\tilde{\nu}}$, derived from $\mu^+\mu^-$ s' distributions. The region above the solid line is excluded.